

# Neuron Activation Coverage: Rethinking Out-of-distribution Detection and Generalization

**Yibing Liu**

City University of Hong Kong  
lyibing112@gmail.com

**Chris Xing Tian**

City University of Hong Kong  
xingtian4-c@my.cityu.edu.hk

**Haoliang Li**

City University of Hong Kong  
haoliang.li1991@gmail.com

**Lei Ma**

The University of Tokyo  
ma.lei@acm.org

**Shiqi Wang**

City University of Hong Kong  
shiqiwang@cityu.edu.hk

## Abstract

The out-of-distribution (OOD) problem generally arises when neural networks encounter data that significantly deviates from the training data distribution, *i.e.*, in-distribution (InD). In this paper, we study the OOD problem from a neuron activation view. We first formulate neuron activation states by considering both the neuron output and its influence on model decisions. Then, we propose the concept of *neuron activation coverage* (NAC), which characterizes the neuron behaviors under InD and OOD data. Leveraging our NAC, we show that 1) InD and OOD inputs can be naturally separated based on the neuron behavior, which significantly eases the OOD detection problem and achieves a record-breaking performance of 0.03% FPR95 on ResNet-50, outperforming the previous best method by 20.67%; 2) a positive correlation between NAC and model generalization ability consistently holds across architectures and datasets, which enables a NAC-based criterion for evaluating model robustness. By comparison with the traditional validation criterion, we show that NAC-based criterion not only can select more robust models, but also has a stronger correlation with OOD test performance.

## 1 Introduction

Recent advances in machine learning systems hinge on an implicit assumption that the training and test data share the same distribution, known as in-distribution (InD) [19, 61, 23, 56]. However, this assumption rarely holds in real-world scenarios, due to the presence of out-of-distribution (OOD) data, *e.g.*, samples pertaining to the unseen classes [8, 9]. Such distribution shifts between OOD and InD often drastically challenge well-trained models, resulting in significant performance drops [50, 15, 24].

Prior efforts tackling this OOD problem mainly arise from two avenues: 1) OOD detection and 2) OOD generalization. The former one targets at designing tools that differentiate between InD and OOD data inputs, thereby refraining from using unreliable model predictions during real-world deployment [42, 43, 25, 38, 59, 29, 12, 30, 18]. In contrast, OOD generalization focuses on developing robust networks to generalize unseen OOD data, though solely leveraging InD data for training [9, 41, 57, 55, 51, 47, 4, 32, 22]. Despite a plethora of studies emerging over this OOD problem, we find that an alternative space – *the behavior of individual neurons* – still leaves under-explored.

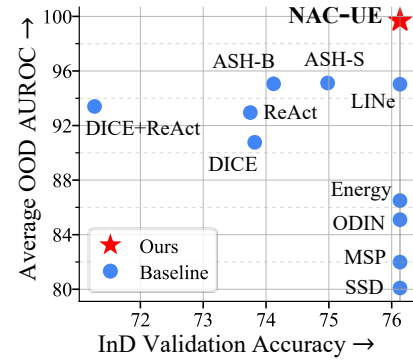


Figure 1: OOD detection performance (AUROC) of NAC-UE on ResNet-50, averaged over 4 datasets. We achieve a record-breaking performance without impairing model classification ability.

As demonstrated in Figure 2, neurons could exhibit distinct activation patterns when exposed to data inputs from InD and OOD. This reveals the potential of leveraging neuron behavior to characterize model states in terms of the OOD problem. Yet, though several studies recognize this significance, they either choose to modify the neural networks [58], or lack the suitable definition of neuron activation states [2, 62]. For instance, [58] proposes a neuron truncation strategy that clips neuron output to separate the InD and OOD data, thereby improving the OOD detection. However, such truncation would unexpectedly decrease the model classification ability [18]. More recently, [2] and [62] employ a threshold to characterize neurons into binary states (*i.e.*, activated or not) based on the neuron output. This characterization, however, discards the valuable neuron distribution details. Unlike them, in this paper, we show that by leveraging natural neuron activation states, a simple statistical property of neuron distribution could effectively facilitate the OOD solutions.

We first propose to formulate the neuron activation state by considering both the neuron output and its influence on model decisions. Specifically, inspired by [29], we model neuron influence as the gradients derived from Kullback-Leibler (KL) divergence [37] between network output and a uniform vector. Then, to characterize the relationship between neuron behavior and the OOD problem, we draw insights from neuron coverage analysis in system testing [48, 44, 67], which reveals that rarely activated (covered) neurons under an input set can potentially trigger undetected defects, *e.g.*, misclassifications. In this sense, we introduce the concept of *neuron activation coverage* (NAC), which quantifies the degree that a neuron state is covered under an InD set. Specifically, if a neuron state is frequently activated by InD data, the NAC score would be high, denoting fewer potential defects that can be triggered under this state. In this work, we apply NAC to two OOD tasks<sup>1</sup>:

**OOD detection.** Since OOD data often trigger abnormal neuron activations, they should present smaller NAC scores compared to the InD input data. As such, we present NAC for Uncertainty Estimation (NAC-UE), which directly averages NAC scores over all neurons as data uncertainty. We evaluate our method across three architectures and benchmarks, establishing a record-breaking performance on the large-scale ImageNet OOD benchmark [16]. Notably, our NAC-UE method achieves a 0.03% FPR95 (99.99% AUROC) on ResNet-50 backbone without impairing model classification ability, which outperforms the previous best method by 20.67% (4.96%) (See Figure 1).

**OOD generalization.** As a larger NAC score could indicate fewer potential defects, we hypothesize that if the whole neuron activation space is fully covered by InD training data, the more robust a neuron would be. To this end, we employ NAC for Model Evaluation (NAC-ME), which measures model generalization ability based on the integral of NAC distribution *w.r.t.* all neurons. Through experiments on DomainBed [22], we find that a positive correlation between NAC and model generalization ability consistently holds across architectures and datasets. Moreover, by comparison with the InD validation criterion, NAC-ME not only can select more robust models, but also strongly correlates with OOD test performance. On the TerraInc dataset, NAC-ME achieves a rank correlation of 34.84% with test accuracy, beating validation criterion by 33.92% on Vit-b16.

## 2 NAC: Neuron Activation Coverage

This paper studies the OOD problem for supervised multi-class learning, where  $\mathcal{X} = \mathbb{R}^d$  denotes the input space and  $\mathcal{Y} = \{1, 2, \dots, C\}$  is the output space. Let  $D_{tr} = \{(\mathbf{x}_i, y_i)\}_{i=1}^{n_t}$  be the training set and  $D_{val} = \{(\tilde{\mathbf{x}}_i, \tilde{y}_i)\}_{i=1}^{n_v}$  be the validation set, both of which are comprised of *i.i.d.* samples from the joint distribution  $\mathcal{P} = \mathcal{X} \times \mathcal{Y}$ . A neural network parameterized by  $\theta$ ,  $F(\mathbf{x}; \theta) : \mathcal{X} \rightarrow \mathbb{R}^{|\mathcal{Y}|}$ , is trained on samples drawn from  $\mathcal{P}$ , producing a logit vector for classification. We denote  $\mathcal{D}_{in}$  as the marginal distribution of  $\mathcal{P}$  over  $\mathcal{X}$ , representing the distribution of InD data. During testing, we will meet out-of-distribution data, which follows a distribution  $\mathcal{D}_{out}$  over  $\mathcal{X}$ .

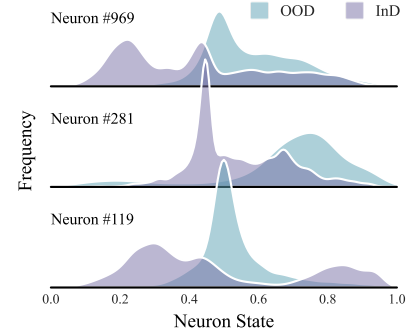


Figure 2: OOD vs. InD neuron activation states. We utilize PACS [39] Photo domain as InD, and Sketch as OOD. All neurons stem from the penultimate layer in ResNet-50.

<sup>1</sup>The code is available at [https://github.com/bierone/ood\\_coverage](https://github.com/bierone/ood_coverage)

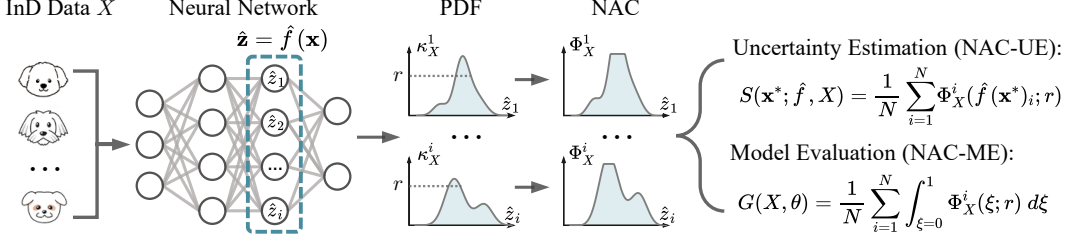


Figure 3: Illustration of our NAC-based methods. Our NAC function is derived from the probability density function (PDF), which quantifies the degree that a neuron state is covered under the InD dataset  $X$ . Building upon NAC, we devise two approaches for tackling different OOD problems: OOD Detection (NAC-UE) and OOD Generalization (NAC-ME).

Figure 3 illustrates our NAC-based approaches. In the following, we first formulate the neuron activation state (Section 2.1), and then introduce the details of our NAC function (Section 2.2). We finally show how to apply NAC to two OOD problems (Section 2.3). See Appendix for more details.

## 2.1 Formulation of Neuron Activation State

Neuron outputs generally depend on the propagation from network input to the layer where the neuron resides. However, this does not consider the neuron influence in subsequent propagations. As such, we introduce gradients backpropagated from the KL divergence between network output and a uniform vector [29], to model the neuron influence. Formally, we denote by  $f(\mathbf{x}) = \mathbf{z} \in \mathbb{R}^N$  the output vector of a specific layer (Section 3.1 discusses this layer choice), where  $N$  is the number of neurons and  $z_i$  is the raw output of  $i$ -th neuron in this layer. By setting the uniform vector  $\mathbf{u} = [1/C, 1/C, \dots, 1/C] \in \mathbb{R}^C$ , the desired KL divergence can be given as:

$$D_{\text{KL}}(\mathbf{u} \parallel \mathbf{p}) = \sum_{i=1}^C u_i \log \frac{u_i}{p_i} = - \sum_{i=1}^C u_i \log p_i - H(\mathbf{u}), \quad (1)$$

where  $\mathbf{p} = \text{softmax}(F(\mathbf{x}))$ , and  $p_i$  denotes  $i$ -element in  $\mathbf{p}$ .  $H(\mathbf{u}) = - \sum_{i=1}^C u_i \log u_i$  is a constant. By combining the KL gradient with neuron output, we then formulate *neuron activation state* as,

$$\hat{\mathbf{z}} = \sigma(\mathbf{z} \odot \frac{\partial D_{\text{KL}}(\mathbf{u} \parallel \mathbf{p})}{\partial \mathbf{z}}), \quad (2)$$

where  $\sigma(x) = 1/(1 + e^{-\alpha x})$  is the sigmoid function with a steepness controller  $\alpha$ . In the rest of this paper, we will also use the notation  $\hat{f}(\mathbf{x}) := \hat{\mathbf{z}}$  to represent the neuron state function.

**Theoretical insights.** We further analyze the gradients from KL divergence to show how this part contributes to the neuron activation state. Without loss of generality, let the predictor following  $\mathbf{z}$  be two fully-connected layers:  $g(\mathbf{z}) = \mathbf{W}_2[\mathbf{W}_1 \mathbf{z}]^+$ , such that  $F = f \circ g$ . Here,  $\mathbf{W}_1 \in \mathbb{R}^{K \times N}$  and  $\mathbf{W}_2 \in \mathbb{R}^{C \times K}$  are two weight matrices, and  $[\cdot]^+$  denotes the ReLU function. For simplicity, the bias term is absorbed into the weight matrices. Since  $F(\mathbf{x}) = g(f(\mathbf{x})) = g(\mathbf{z})$ , we have  $\partial F(\mathbf{x})/\partial \mathbf{z} = \partial g(\mathbf{z})/\partial \mathbf{z} = (\mathbf{W}_1^T \mathbf{M}) \mathbf{W}_2^T$ , where  $\mathbf{M} = \text{diag}(1_{\mathbf{W}_1 \mathbf{z} > 0})$  is the gradient mask of ReLU function. The neuron activation state thus can be given as:

$$\hat{\mathbf{z}} = \sigma(\mathbf{z} \odot \frac{\partial D_{\text{KL}}}{\partial \mathbf{z}}) = \sigma(\mathbf{z} \odot (\frac{\partial g(\mathbf{z})}{\partial \mathbf{z}} \cdot \frac{\partial D_{\text{KL}}}{\partial g(\mathbf{z})})) = \sigma(\mathbf{z} \odot (\overbrace{(\mathbf{W}_1^T \mathbf{M}) \mathbf{W}_2^T}^{\text{relevance to output space}} \cdot \overbrace{(\mathbf{p} - \mathbf{u})}^{\text{sample confidence}})), \quad (3)$$

where  $\partial D_{\text{KL}}/\partial g(\mathbf{z}) = (\mathbf{p} - \mathbf{u})$  measures how model predictions deviate from a uniform distribution, thus denoting sample confidence [29]. As shown above, we build neuron activation state from three perspectives: 1) the magnitude of raw neuron output  $\mathbf{z}$ , 2) the neuron relevance to output space; and 3) the model confidence on the input. Intuitively, if a neuron is not relevant to the output (or the model is not confident about the input), the neuron would be considered less active during propagation.

## 2.2 Neuron Activation Coverage (NAC) Function

With the formulation of neuron activation state, we now introduce the *neuron activation coverage* (NAC) function to characterize the neuron behaviors under InD and OOD data. Inspired by system testing [48, 44, 67], NAC aims to quantify the degree that a neuron state is covered under an InD

dataset. The intuition is that *if a neuron state is rarely activated (covered) by any InD input, the chances of triggering bugs (e.g., misclassification) under this state would be high*. Since NAC directly measures the statistical property (*i.e.*, coverage) of distribution *w.r.t.* neuron states, we derive the NAC function from the probability density function (PDF). Formally, given a state  $\hat{z}_i$  of  $i$ -th neuron, and its PDF  $\kappa_X^i(\cdot)$  over an InD set  $X$ , the function for NAC can be given as:

$$\Phi_X^i(\hat{z}_i; r) = \frac{1}{r} \min(\kappa_X^i(\hat{z}_i), r), \quad (4)$$

where  $\kappa_X^i(\hat{z}_i)$  is the probability density of  $\hat{z}_i$  over the set  $X$ , and  $r$  denotes the lower bound for achieving full coverage *w.r.t.* state  $\hat{z}_i$ . In cases where the neuron state  $\hat{z}_i$  is frequently activated by InD data, the NAC score  $\Phi_X^i(\hat{z}_i; r)$  would be 1, denoting fewer potential defects that can be triggered under this state. Notably, if  $r$  is too low, noisy activations would dominate the coverage, reducing the significance of NAC scores. Conversely, an excessively large value of  $r$  also makes the NAC function vulnerable to data biases. For example, given a homogeneous dataset comprising numerous similar samples, the NAC score of a specific neuron state can be easily mischaracterized as abnormally high, marginalizing the effects of other meaningful states. We analyze the effect of  $r$  in Section 3.1.

### 2.3 Applications

After modeling the NAC function over InD data, we can directly apply it to tackle existing OOD problems. In the following, we illustrate two application scenarios.

**Uncertainty estimation for OOD detection.** Since OOD data often trigger abnormal neuron behaviors (corresponding to small NAC scores), we employ NAC for **Uncertainty Estimation** (NAC-UE), which directly average NAC scores over all neurons as the uncertainty of input samples. Formally, given a test data  $\mathbf{x}^*$ , the function for NAC-UE can be given as,

$$S(\mathbf{x}^*; \hat{f}, X) = \frac{1}{N} \sum_{i=1}^N \Phi_X^i(\hat{f}(\mathbf{x}^*)_i; r), \quad (5)$$

where  $N$  is the number of neurons;  $\hat{f}(\mathbf{x}^*)_i := \hat{z}_i$  denotes the activation state of  $i$ -th neuron;  $r$  is the controller of NAC function. In particular, if the neuron states triggered by  $\mathbf{x}^*$  are frequently activated by InD samples, the coverage score  $S(\mathbf{x}^*; \hat{f}, X)$  would be high, suggesting that  $\mathbf{x}^*$  is likely to come from InD distribution. As such, we propose using NAC-UE for OOD detection following [2, 29, 58, 43]:

$$D(\mathbf{x}^*) = \begin{cases} \text{InD} & \text{if } S(\mathbf{x}^*; \hat{f}, X) \geq \lambda; \\ \text{OOD} & \text{if } S(\mathbf{x}^*; \hat{f}, X) < \lambda, \end{cases} \quad (6)$$

where  $\lambda$  is a threshold. The sample with an uncertainty score  $S(\mathbf{x}^*; \hat{f}, X)$  less than  $\lambda$  would be categorized as OOD (*i.e.*,  $\mathbf{x}^* \in \mathcal{D}_{out}$ ); otherwise, InD (*i.e.*,  $\mathbf{x}^* \in \mathcal{D}_{in}$ ).

**Model evaluation for OOD generalization.** As a larger NAC score could indicate fewer potential defects, we hypothesize that if the whole neuron activation space is fully covered by InD data, the more robust a neuron would be. In this sense, we propose **NAC for Model Evaluation** (NAC-ME), which characterizes model generalization ability based on the integral of NAC distribution *w.r.t.* all neurons. Formally, given an InD dataset  $X$ , NAC-ME measures the generalization ability of a model (parameterized by  $\theta$ ) as the average of integral *w.r.t.* NAC distribution:

$$G(X, \theta) = \frac{1}{N} \sum_{i=1}^N \int_{\xi=0}^1 \Phi_X^i(\xi; r) d\xi, \quad (7)$$

where  $N$  is the number of neurons, and  $r$  is the controller of NAC function. Specifically, if a neuron is consistently active on the whole activation space (*i.e.*, high NAC integral), we consider the probability that it meets bugs would be lower, indicating favorable robustness.

**Approximation.** Our approach supports mini-batch approximation, allowing for efficient processing of large datasets. We utilize the typical histogram-based approach to model PDF, which divides the neuron activation space into  $M$  equally-spaced intervals. In this way, mini-batch approximation

Method	iNaturalist [27]		SUN [66]		Places [72]		Textures [14]		Average	
	FPR95 ↓	AUROC ↑	FPR95 ↓	AUROC ↑	FPR95 ↓	AUROC ↑	FPR95 ↓	AUROC ↑	FPR95 ↓	AUROC ↑
<i>Backbone: ResNet-50</i>										
MSP [25]	54.99	87.74	70.83	80.86	73.99	79.76	68.00	79.61	66.95	81.99
ODIN [42]	47.66	89.66	60.15	84.59	67.89	81.78	50.23	85.62	56.48	85.41
Mahalanobis [38]	97.00	52.65	98.50	42.41	98.40	41.79	55.80	85.01	87.43	55.47
Energy [43]	55.72	89.95	59.26	85.89	64.92	82.86	53.72	85.99	58.41	86.17
SSD [53]	57.16	87.77	78.23	73.10	81.19	70.97	36.37	88.52	63.24	80.09
DICE [59]	25.63	94.49	35.15	90.83	46.49	87.48	31.72	90.30	34.75	90.77
DICE+ReAct [59]	18.64	96.24	25.45	93.94	36.86	90.67	28.07	92.74	27.25	93.40
ASH-B [18]	14.21	97.32	22.08	95.10	33.45	92.31	21.17	95.50	22.73	95.06
LINe [2]	12.26	97.56	19.48	95.26	28.52	92.85	22.54	94.44	20.70	95.03
<b>NAC-UE (Ours)</b>	<b>0.00<sub>±0.00</sub></b>	<b>100.00<sub>±0.00</sub></b>	<b>0.01<sub>±0.01</sub></b>	<b>99.99<sub>±0.00</sub></b>	<b>0.09<sub>±0.01</sub></b>	<b>99.97<sub>±0.00</sub></b>	<b>0.01<sub>±0.01</sub></b>	<b>100.00<sub>±0.00</sub></b>	<b>0.03</b>	<b>99.99</b>
<i>Backbone: BiTS-R101x1</i>										
MSP [25]	63.69	87.59	79.98	78.34	81.44	76.76	82.73	74.45	76.96	79.29
ODIN [42]	62.69	89.36	71.67	83.92	76.27	80.67	81.31	76.30	72.99	82.56
Mahalanobis [38]	96.34	46.33	88.43	65.20	89.75	64.46	52.23	72.10	81.69	62.02
Energy [43]	64.91	88.48	65.33	85.32	73.02	81.37	80.87	75.79	71.03	82.74
KL Matching [11]	27.36	93.00	67.52	78.72	72.61	76.49	49.70	87.07	54.30	83.82
GradNorm [29]	50.03	90.33	46.48	89.03	60.86	84.82	61.42	81.07	54.70	86.31
MOS [30]	9.28	98.15	40.63	92.01	49.54	89.06	60.43	81.23	39.97	90.11
<b>NAC-UE (Ours)</b>	<b>0.01<sub>±0.00</sub></b>	<b>100.00<sub>±0.00</sub></b>	<b>0.06<sub>±0.01</sub></b>	<b>99.98<sub>±0.00</sub></b>	<b>0.07<sub>±0.02</sub></b>	<b>99.98<sub>±0.00</sub></b>	<b>1.22<sub>±0.04</sub></b>	<b>99.58<sub>±0.00</sub></b>	<b>0.34</b>	<b>99.88</b>
<i>Backbone: MobileNet-v2</i>										
MSP [25]	64.29	85.32	77.02	77.10	79.23	76.27	73.51	77.30	73.51	79.00
ODIN [42]	55.39	87.62	54.07	85.88	57.36	84.71	49.96	85.03	54.20	85.81
Mahalanobis [38]	62.11	81.00	47.82	86.33	52.09	83.63	92.38	33.06	63.60	71.01
Energy [43]	59.50	88.91	62.65	84.50	69.37	81.19	58.05	85.03	62.39	84.91
DICE [59]	43.09	90.83	38.69	90.46	53.11	85.81	32.80	91.30	41.92	89.60
DICE+ReAct [59]	32.30	93.57	31.22	92.86	46.78	88.02	16.28	96.25	31.64	92.68
ASH-B [18]	31.46	94.28	38.45	91.61	51.80	87.56	20.92	95.07	35.66	92.13
LINe [2]	24.95	95.53	33.19	92.94	47.95	88.98	12.30	97.05	29.60	93.62
<b>NAC-UE (Ours)</b>	<b>0.00<sub>±0.00</sub></b>	<b>100.00<sub>±0.00</sub></b>	<b>0.00<sub>±0.00</sub></b>	<b>100.00<sub>±0.00</sub></b>	<b>0.02<sub>±0.00</sub></b>	<b>100.00<sub>±0.00</sub></b>	<b>0.85<sub>±0.03</sub></b>	<b>99.84<sub>±0.00</sub></b>	<b>0.22</b>	<b>99.96</b>

Table 1: OOD detection results on ImageNet. We report the performance over three backbones, which are trained solely on the InD dataset, *i.e.*, ImageNet-1k.  $\uparrow$  denotes the higher value is better, while  $\downarrow$  indicates lower values are better. The results of our methods are averaged over 20 random seeds.

iteratively takes a random batch of neuron states as input and assigns them corresponding intervals. Furthermore, we efficiently calculate  $G(X, \theta)$  based on the Riemann approximation [36],

$$G(X, \theta) = \frac{1}{MN} \sum_{i=1}^N \sum_{k=1}^M \Phi_X^i\left(\frac{k}{M}; r\right). \quad (8)$$

### 3 Experiments

In this section, we evaluate our approaches on two tasks: OOD detection (NAC-UE) (Section 3.1) and OOD generalization (NAC-ME) (Section 3.2). We provide more details in Appendix.

#### 3.1 Case Study 1: OOD Detection

**Setup.** Our experimental settings align with previous SoTAs [58, 29, 18, 2, 30, 43]. We mainly evaluate our NAC-UC on the large-scale ImageNet benchmark [30], where ImageNet-1k serves as the InD dataset, along with 4 OOD test datasets: iNaturalist [27], SUN [66], Places365 [48] [72], and Textures [14], which consist of non-overlapping categories with ImageNet-1k. In this series of experiments, we utilize the pretrained ResNet-50 [23], MobileNet-v2 [52], and Google BiTS-R101x1 [35] as backbones following [18, 58, 29]. Additionally, we run experiments on CIFAR-10 and CIFAR-100, where the InD dataset corresponds to CIFAR, and 6 OOD datasets are included: SVHN [46], LSUN-Crop [70], LSUN-Resize [70], iSUN [68], Places365 [72], and Textures [14]. We employ ResNet-18 in CIFAR following [58]. Detailed results are provided in Appendix.

We utilize two threshold-free metrics in our evaluation: 1) FPR95: the false-positive-rate of OOD samples when the true positive rate of ID samples is at 95%; 2) AUROC: the area under the receiver operating characteristic curve. Throughout our experiments, all pretrained models are left unmodified, preserving their classification ability during the OOD detection phase.

**Implementation details.** In all of our experiments, we first utilize the InD dataset to model the NAC function, and then apply NAC-UE to calculate uncertainty scores during the test phase (See Eq. (5)).

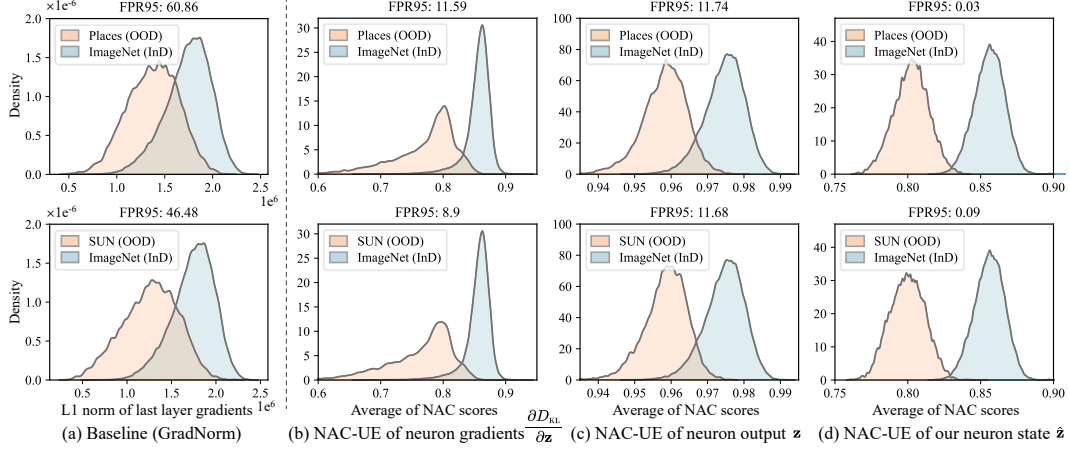


Figure 4: Ablation studies on the form of neuron activation state. We visualize the distributions of uncertainty scores *w.r.t.* (a) GradNorm baseline [29] utilizing the L1 norm of KL gradients in the last layer; (b) NAC-UE regarding the KL gradients of neuron output,  $\partial D_{KL} / \partial \mathbf{z}$ ; (c) NAC-UE *w.r.t.* raw neuron output,  $\mathbf{z}$ ; (d) NAC-UE of defined neuron state,  $\hat{\mathbf{z}}$ . The results are based on BiTS-R101x1.

Method	CIFAR-10		CIFAR-100	
	FPR95 ↓	AUROC ↑	FPR95 ↓	AUROC ↑
MSP [25]	56.71	91.17	80.72	76.83
ODIN [42]	31.10	93.79	66.21	82.88
Energy [43]	35.60	93.57	71.93	82.82
ReAct [58]	32.91	94.27	59.61	87.48
NAC-UE (Ours)	<b>0.16</b>	<b>99.95</b>	<b>0.20</b>	<b>99.94</b>

Table 2: OOD detection results on CIFAR-10 and CIFAR-100. We utilize ResNet-18 as backbone. Results are averaged on 20 seeds over 6 OOD datasets. Detailed scores are provided in Appendix.

We set  $r = 0.6$  and  $M = 30000$  for MobileNet-v2; otherwise,  $r = 1$  and  $M = 10000$ . For all pretrained models, we set  $\alpha = 1000$ , and calculate NAC-UE for neurons from the penultimate layer.

**Results.** As illustrated in Table 1, we first compare our approach with recent SoTAs on ImageNet benchmark, where our NAC-UE consistently outperforms previous methods on 4 OOD datasets, and establishes a record-breaking performance over 3 pretrained models. More importantly, NAC-UE reduces the FPR95 by 20.67% and 29.38% compared with the previous best method LINe [2] on ResNet-50 and MobileNet-v2, respectively. It also reduces the FPR95 by 39.63% compared with the previous SOTA MOS [30] on BiTS-R101x1. Besides, as previously shown in Figure 1, NAC-UE preserves model classification ability (*i.e.*, InD validation accuracy) during the OOD detection phase, since it performs in a *post-hoc* fashion. In contrast, advanced methods such as ReAct [58] and ASH-B [18] exhibit promising OOD detection results at the expense of InD accuracy.

We further compare NAC-UE with previous SoTAs on CIFAR benchmarks, and the results (averaged over 6 OOD datasets) are illustrated in Table 2. As can be seen, NAC-UE consistently outperforms previous methods across two benchmarks, and showcases the large gains. This highlights the superiority of our method again. We provide detailed performance for each OOD dataset in Appendix.

**The superiority of neuron activation state  $\hat{\mathbf{z}}$ .** In Section 2.1, we formulate the neuron activation state  $\hat{\mathbf{z}}$  by combining the raw neuron output  $\mathbf{z}$  with its KL gradients  $\partial D_{KL} / \partial \mathbf{z}$ . Here, we ablate this formulation to investigate the superiority of  $\hat{\mathbf{z}}$ . In particular, we analyze the NAC-UE *w.r.t.* 1) raw neuron output:  $\mathbf{z}$ , 2) KL gradients of neuron output:  $\partial D_{KL} / \partial \mathbf{z}$ , and 3) our defined neuron state:  $\hat{\mathbf{z}}$ . We also include the baseline GradNorm [29] for a further comparison, which employs the L1 norm of KL gradients in the last layer as uncertainty scores. Figure 4 illustrates the results, where we visualize the distribution of uncertainty scores *w.r.t.* these methods on ImageNet benchmark. We provide the main observations in the following:

Layer	# Neurons	FPR95 ↓	AUROC ↑
Conv1	64	48.26	84.90
Layer1	256	13.59	97.67
Layer2	512	16.76	97.41
Layer3	1024	<b>0.02</b>	99.94
Layer4	2048	0.03	<b>99.99</b>

Table 3: Effect of NAC-UE using neurons from different layers. We report averaged scores on ImageNet benchmark by utilizing ResNet-50 backbone.

Firstly, we can observe that all NAC-based methods significantly outperform the baseline GradNorm. Specifically, the distribution between the InD and OOD samples could be largely separated when using NAC as uncertainty scores, thereby leading to the the lower FPR95. Secondly, among all the three variants of NAC-UE,  $\hat{\mathbf{z}}$ -based method performs the best, as it inherits the advantages from both  $\mathbf{z}$  and  $\partial D_{KL} / \partial \mathbf{z}$ . This spotlights the superiority of our defined neuron state. Thirdly, it can also be found that OOD samples generally present lower neuron activation coverage compared to InD samples. This demonstrates that OOD data tend to provoke abnormal neuron behaviors in comparison to InD data, which further confirms the rationale behind our NAC-based approaches.

**Where to apply neuron action coverage (NAC)?** Prior studies have shown that the neurons from deeper layers often encode rich semantic information [6, 26]. Inspired by this, our experiments mostly implement NAC-UE by utilizing neurons from the penultimate layer. Here, we take ResNet-50 as backbone and analyze this layer choice. As shown in Table 3, we compare the OOD detection results of NAC-UE *w.r.t.* different layer choices. It can be drawn that as the layer goes deeper, more neuron numbers are considered, along with improved detection performance. Moreover, we can also observe that even with a single layer of neurons, NAC-UE is able to achieve favorable performance, which eases its integration into other architectures.

Sigmoid Steepness ( $\alpha$ )	FPR95 ↓	AUROC ↑
$\alpha = 100$	94.24	46.75
$\alpha = 500$	35.34	92.80
$\alpha = 1000$	<b>0.34</b>	<b>99.88</b>
$\alpha = 5000$	8.41	98.29
$\alpha = 8000$	14.44	96.94

Table 4: The effect of different  $\alpha$  over BiTS-R101x1 backbone.

Lower Bound ( $r$ )	FPR95 ↓	AUROC ↑
$r = 0.25$	71.28	80.91
$r = 1$	<b>0.34</b>	<b>99.88</b>
$r = 2$	2.26	98.85
$r = 10$	34.78	87.68
$r = 100$	75.60	77.02

Table 5: The effect of different  $r$  over BiTS-R101x1.

No. of Intervals ( $M$ )	FPR95 ↓	AUROC ↑
$M = 10$	56.81	81.49
$M = 100$	44.58	89.61
$M = 1000$	42.86	89.35
$M = 5000$	24.09	94.33
$M = 10000$	<b>0.34</b>	<b>99.88</b>

Table 6: The effect of different  $M$  over BiTS-R101x1.

**Paramter analysis.** In Table 4-6, we systematically analyze the effect of sigmoid steepness ( $\alpha$ ), lower bound ( $r$ ) for full coverage, and the number of intervals ( $M$ ) for PDF approximation. The following observations can be noted: 1) A relatively steep sigmoid function could make NAC-UE perform better. We conjecture this is due to that neuron activation states often distribute in a small range, thus requiring a steeper function to distinguish their finer variations; 2) NAC-UE is sensitive to the choice of  $r$ . As previously discussed, if  $r$  is too small, noisy activations can dominate the coverage, thus diminishing the effect of NAC scores. Also, a large  $r$  makes the NAC function susceptible to data biases, *e.g.*, in datasets with numerous similar samples, a neuron state can be easily mischaracterized by an abnormally high NAC score, thereby marginalizing other meaningful neuron states. 3) The performance of NAC-UE positively correlates with  $M$ . This is intuitive as a larger  $M$  allows for a closer approximation to the real PDF, resulting in improved performance.

### 3.2 Case Study 2: OOD Generalization

**Setup.** Our experimental settings carefully follow the Domainbed benchmark [22]. Without employing digital images, we adopt four datasets: VLCS [20] (4 domains, 10,729 images), PACS [39] (4 domains, 9,991 images), OfficeHome [65] (4 domains, 15,588 images), and TerraInc [7] (4 domains, 24,788 images). For all datasets, we report the *leave-one-out* test accuracy following [22], whereby results are averaged over cases that use a single domain for test and the others for training. For all employed backbones, we utilize the hyperparameters suggested by [10] to fine-tune them. The training strategy is ERM [64], unless stated otherwise. We set the total training steps as 5000, and the evaluation frequency as 300 steps for all models. We provide implementation details in Appendix.

**Model evaluation criteria.** Since OOD data is assumed unavailable during model training, existing methods commonly resort to InD validation accuracy to evaluate a model [49, 32, 69, 55, 22]. Thus, we mainly compare our NAC-ME with the prevalent *validation criterion* [22]. We also leverage the *oracle criterion* [22] as the upper bound, which directly utilizes OOD test data to evaluate a model.

**Metrics.** We utilize two metrics in this setting: 1) Spearman Rank Correlation (RC) between OOD test accuracy and the model evaluation scores (*i.e.*, InD validation accuracy or InD NAC scores), which are sampled at regular evaluation intervals (*i.e.*, every 300 steps) during the training process; 2) OOD Test Accuracy (ACC) of the best model selected by the criterion within a single run of training.

Bakbone	Method	VLCS [20]		PACS [39]		OfficeHome [65]		TerraInc [7]		Average	
		RC	ACC	RC	ACC	RC	ACC	RC	ACC	RC	ACC
ResNet-18	Oracle	-	77.17	-	80.13	-	56.00	-	44.32	-	64.40
	Validation	34.27	75.12	68.71	79.01	83.50	55.60	38.77	39.03	56.31	62.19
	NAC-ME	<b>52.00</b>	<b>76.10</b>	<b>72.55</b>	<b>79.12</b>	<b>84.78</b>	<b>55.80</b>	<b>39.28</b>	<b>40.41</b>	<b>62.15</b>	<b>62.86</b>
ResNet-50	Oracle	-	79.67	-	85.41	-	65.14	-	50.23	-	70.21
	Validation	<b>31.43</b>	<b>77.70</b>	58.54	84.57	67.93	65.04	37.07	46.07	48.74	68.34
	NAC-ME	28.78	76.69	<b>61.52</b>	<b>84.89</b>	<b>69.24</b>	<b>65.14</b>	<b>40.95</b>	<b>47.18</b>	<b>50.12</b>	<b>68.48</b>
Vit-t16	Oracle	-	78.4	-	71.83	-	61.25	-	41.08	-	63.14
	Validation	40.63	77.55	88.42	69.77	98.47	<b>61.09</b>	22.71	36.28	62.56	61.17
	NAC-ME	<b>45.26</b>	<b>77.68</b>	<b>90.22</b>	<b>71.14</b>	<b>98.82</b>	60.97	<b>23.82</b>	<b>37.47</b>	<b>64.53</b>	<b>61.82</b>
Vit-b16	Oracle	-	80.44	-	89.10	-	80.84	-	51.81	-	75.55
	Validation	29.94	<b>79.14</b>	31.54	86.86	65.24	80.45	0.92	45.49	31.91	72.99
	NAC-ME	<b>33.76</b>	79.05	<b>40.30</b>	<b>88.19</b>	<b>68.38</b>	<b>80.65</b>	<b>34.84</b>	<b>46.51</b>	<b>44.32</b>	<b>73.60</b>
	$\Delta$	(+3.82)	(-0.09)	(+8.76)	(+1.33)	(+3.15)	(+0.20)	(+33.92)	(+1.02)	(+12.41)	(+0.61)

Table 7: OOD generalization results on DomainBed. *Oracle* indicates the upper bound, which utilizes OOD test data to evaluate a model.  $\Delta$  denotes the improvement of coverage criterion over the validation criterion. The training strategy is ERM [64]. All scores are averaged over 3 random trials.

Algorithm	Method	RC	ACC
SelfReg [32]	Oracle	-	83.64
	Validation	61.76	80.66
	NAC-ME	<b>64.50</b>	<b>80.95</b>
CORAL [57]	Oracle	-	84.40
	Validation	70.06	80.68
	NAC-ME	<b>75.53</b>	<b>81.19</b>
	$\Delta$	(+5.47)	(+0.51)

Table 8: OOD generalization results on PACS [39], averaged over 3 random trials.  $\Delta$  denotes the improvement of coverage criterion over the validation. Backbone: ResNet-18.

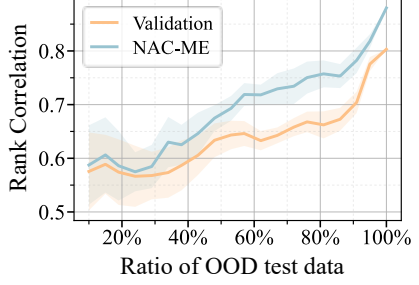


Figure 5: The positive relationship between rank correlation (RC) and the volume of OOD test data. Results are based on iWild-CAM [34]. Backbone: ResNet-50.

**Results.** As illustrated in Table 7, we mainly compare our NAC-ME with typical validation criterion over four canonical backbones: ResNet-18 [23], ResNet-50 [23], Vit-t16 [19], and Vit-b16 [19]. Throughout the results, we can draw the following observations: 1) The positive correlation (*i.e.*,  $RC > 0$ ) between the NAC scores and the OOD test performance consistently holds across architectures and datasets; 2) By comparison with the validation criterion, NAC-ME not only could select more generalized models (with higher OOD accuracy), but also exhibits stronger correlation with OOD test performance. For instance, on the TerraInc dataset, NAC-ME achieves a rank correlation of 34.84% with OOD test accuracy, surpassing validation criterion by 33.92% on the Vit-b16. Similarly, on the VLCS dataset, NAC-ME also shows a rank correlation of 52.00%, outperforming the validation criterion by 17.73% on the ResNet-18. Such results highlight the potential of leveraging our neuron activation coverage to reflect model generalization ability.

**Can NAC co-work with SoTA learning algorithms?** Recent literature has suggested numerous learning algorithms to enhance the model generalization ability [57, 21, 55, 49]. In this sense, we further investigate the potential of NAC-ME by implementing it with two recent SoTA algorithms: SelfReg [32] and CORAL [57]. The results are shown in Table 8. It can be found that NAC-ME as an evaluation criterion still presents better performance compared with validation criterion. This finding further verifies the effectiveness of our NAC-based criterion.

**Does the volume of OOD test data hinder the Rank Correlation (RC)?** As illustrated in Table 7, while in most cases NAC-ME outperforms the validation criterion on model selection, we can find that the Rank Correlation (RC) still falls short of its maximum value, *e.g.*, on the VLCS dataset using ResNet-18, RC only reaches 52% compared to the maximum of 100%. Given that Domainbed only provides 6 OOD domains at most, we hypothesize that the volume/variance of OOD test data

may be the reason: insufficient OOD test data may be unreliable to reflect model generalization ability, thereby hindering the validity of RC. To this end, we conduct additional experiments on the iWildCam dataset [34], which includes 323 domains and 203,029 images in total. Figure 5 illustrates the results, where we analyze the relationship between RC and the volume of OOD test data by randomly sampling different ratios of OOD data for RC calculation. As can be seen, an increase in the ratio of test data also leads to an improvement in the RC, which confirms our hypothesis regarding the effect of OOD data. Furthermore, we can observe that in most cases, NAC-ME could still outperform the validation criterion. These observations spotlight the capability of our NAC again.

## 4 Related Work

**Neuron coverage.** Traditional system testing commonly leverages coverage criteria to uncover defects in software programs [3]. These criteria directly measure the degree to which certain codes or components have been exercised, thereby indicating potential defects. To simulate such program testing in deep neural networks, Pei *et al.* [48] firstly introduced neuron coverage, which measures the proportion of activated neurons within a given input set. The underlying idea is that if a network performs with larger neuron coverage during testing, there would be fewer undetected bugs (*e.g.*, misclassification) that can be triggered. In line with this, Ma *et al.* [44] extended the neuron coverage with fine-grained criteria, which further considers the distribution of neuron outputs from training data. Subsequently, Yuan *et al.* [71] advocated focusing on the interactions between neurons within the same layer, and introduced a layer-wise neuron coverage for network testing. The most recent work related to our paper is [62], where they proposed to improve model generalization ability by maximizing neuron coverage during training. Likewise, in this work, we also demonstrate that the InD neuron activation coverage can be a potential criterion for evaluating model robustness, which even could surpass prevalent validation criterion across architectures and datasets.

**OOD detection.** The goal of OOD detection is to distinguish between InD and OOD data inputs, thereby refraining from using unreliable model predictions during deployment. Existing detection methods can be broadly categorized into three groups: 1) confidence-based [42, 8, 25, 30, 17], 2) distance-based [28, 13, 63, 45, 60, 38], and 3) density-based [1, 73, 31, 33] approaches. Confidence-based methods commonly resort to the confidence level of model outputs to detect OOD samples. For example, MSP [25] directly calculates the maximum softmax probability as the uncertainty score. In contrast, distance-based approaches identify OOD samples by measuring the distance (*e.g.*, Mahalanobis distance [38]) between input sample and typical InD centroids or prototypes. Likewise, density-based methods employ probabilistic models to explicitly model InD distribution, and classify test data located in low-density regions as OOD.

Specific to neuron behaviors, ReAct [58] recently proposes to truncate high neuron activations to separate the InD and OOD data. However, such truncation would instead decrease model classification ability [18]. Similarly, LINe [2] seeks to find important neurons based on the Shapley value [54] and then performs activation clipping. Yet, this approach relies on a threshold-based strategy that categorizes neurons into binary states (*i.e.*, activated or not), thus disregarding valuable neuron distribution details. Unlike them, in this work, we show that by using natural neuron states, a distribution property (*i.e.*, coverage) could greatly facilitate the OOD detection.

**OOD generalization.** OOD generalization aims to train models that can overcome distribution shifts between InD and OOD data. While a myriad of studies has emerged to tackle this problem [41, 57, 51, 47, 4, 21, 40], Gulrajani *et al.* [22] recently put forth the importance of model evaluation criterion, and demonstrated that a vanilla ERM [64] along with a proper criterion could outperform most state-of-the-art methods. In line with this, Arpit *et al.* [5] discovered that using validation accuracy as the evaluation criterion could be unstable for model selection, and thus proposed moving average to stabilize model training. Contrary to that, this work sheds light on the potential of neuron activation coverage for model evaluation, showing that it outperforms the validation criterion in various cases.

## 5 Conclusion

In this work, we have presented a neuron activation view to reflect the OOD problem. We have shown that through our formulated neuron states, the concept of neuron activation coverage (NAC) could effectively facilitate two OOD tasks: OOD detection and OOD generalization. Specifically, we have demonstrated that 1) InD and OOD inputs can be more separable based on the neuron activation

coverage, yielding substantially improved OOD detection performance; 2) a positive correlation between NAC and model generalization ability consistently holds across architectures and datasets, which highlights the potential of NAC-based criterion for model evaluation. Along these lines, we hope this paper has further motivated the community to consider neuron behavior in the OOD problem. This is also the most considerable benefit eventually lies.

**Limitation.** The approximation of PDF function can be the limitation. While increasing the number of intervals improves the approximation, it also adds a computational burden. Besides, though using a parametric PDF alleviate this issue, it can be challenging to generalize across model architectures.

## References

- [1] Davide Abati, Angelo Porrello, Simone Calderara, and Rita Cucchiara. Latent space autoregression for novelty detection. In *CVPR*, pages 481–490. IEEE, 2019.
- [2] Yong Hyun Ahn, Gyeong-Moon Park, and Seong Tae Kim. Line: Out-of-distribution detection by leveraging important neurons. In *CVPR*. IEEE, 2023.
- [3] Paul Ammann and Jeff Offutt. *Introduction to Software Testing*. Cambridge University Press, 2008.
- [4] Martín Arjovsky, Léon Bottou, Ishaan Gulrajani, and David Lopez-Paz. Invariant risk minimization. *arXiv preprint arXiv:1907.02893*, 2019.
- [5] Devansh Arpit, Huan Wang, Yingbo Zhou, and Caiming Xiong. Ensemble of averages: Improving model selection and boosting performance in domain generalization. In *NeurIPS*, 2022.
- [6] David Bau, Jun-Yan Zhu, Hendrik Strobelt, Àgata Lapedriza, Bolei Zhou, and Antonio Torralba. Understanding the role of individual units in a deep neural network. *Proc. Natl. Acad. Sci.*, 117(48):30071–30078, 2020.
- [7] Sara Beery, Grant Van Horn, and Pietro Perona. Recognition in terra incognita. In *ECCV*, pages 472–489. Springer, 2018.
- [8] Abhijit Bendale and Terrance E. Boult. Towards open set deep networks. In *CVPR*, pages 1563–1572. IEEE, 2016.
- [9] Gilles Blanchard, Gyemin Lee, and Clayton Scott. Generalizing from several related classification tasks to a new unlabeled sample. In *NeurIPS*, pages 2178–2186, 2011.
- [10] Junbum Cha, Sanghyuk Chun, Kyungjae Lee, Han-Cheol Cho, Seunghyun Park, Yunsung Lee, and Sungrae Park. SWAD: domain generalization by seeking flat minima. In *NeurIPS*, pages 22405–22418, 2021.
- [11] Robin Chan, Krzysztof Lis, Svenja Uhlemeyer, Hermann Blum, Sina Honari, Roland Siegwart, Pascal Fua, Mathieu Salzmann, and Matthias Rottmann. Segmentmeifyoucan: A benchmark for anomaly segmentation. In *NeurIPS Datasets and Benchmarks*, 2021.
- [12] Jiefeng Chen, Yixuan Li, Xi Wu, Yingyu Liang, and Somesh Jha. ATOM: robustifying out-of-distribution detection using outlier mining. In *ECML*, pages 430–445. Springer, 2021.
- [13] Xingyu Chen, Xuguang Lan, Fuchun Sun, and Nanning Zheng. A boundary based out-of-distribution classifier for generalized zero-shot learning. In *ECCV*, pages 572–588. Springer, 2020.
- [14] Mircea Cimpoi, Subhransu Maji, Iasonas Kokkinos, Sammy Mohamed, and Andrea Vedaldi. Describing textures in the wild. In *CVPR*, pages 3606–3613. IEEE, 2014.
- [15] Alexander D’Amour, Katherine A. Heller, Dan Moldovan, Ben Adlam, Babak Alipanahi, Alex Beutel, Christina Chen, Jonathan Deaton, Jacob Eisenstein, Matthew D. Hoffman, Farhad Hormozdiari, Neil Houlsby, Shaobo Hou, Ghassen Jerfel, Alan Karthikesalingam, Mario Lucic, Yi-An Ma, Cory Y. McLean, Diana Mincu, Akinori Mitani, Andrea Montanari, Zachary Nado, Vivek Natarajan, Christopher Nielson, Thomas F. Osborne, Rajiv Raman, Kim Ramasamy, Rory Sayres, Jessica Schrouff, Martin Seneviratne, Shannon Sequeira, Harini Suresh, Victor Veitch, Max Vladymyrov, Xuezhi Wang, Kellie Webster, Steve Yadlowsky, Taedong Yun, Xiaohua Zhai, and D. Sculley. Underspecification presents challenges for credibility in modern machine learning. *arXiv preprint arXiv:2011.03395*, 2020.
- [16] Jia Deng, Wei Dong, Richard Socher, Li-Jia Li, Kai Li, and Li Fei-Fei. Imagenet: A large-scale hierarchical image database. In *CVPR*, pages 248–255. IEEE, 2009.
- [17] Terrance DeVries and Graham W. Taylor. Learning confidence for out-of-distribution detection in neural networks. *arXiv preprint arXiv:1802.04865*, 2018.

[18] Andrija Djurisic, Nebojsa Bozanic, Arjun Ashok, and Rosanne Liu. Extremely simple activation shaping for out-of-distribution detection. In *ICLR*, 2023.

[19] Alexey Dosovitskiy, Lucas Beyer, Alexander Kolesnikov, Dirk Weissenborn, Xiaohua Zhai, Thomas Unterthiner, Mostafa Dehghani, Matthias Minderer, Georg Heigold, Sylvain Gelly, Jakob Uszkoreit, and Neil Houlsby. An image is worth 16x16 words: Transformers for image recognition at scale. In *ICLR*, 2021.

[20] Chen Fang, Ye Xu, and Daniel N. Rockmore. Unbiased metric learning: On the utilization of multiple datasets and web images for softening bias. In *ICCV*, pages 1657–1664. IEEE, 2013.

[21] Yaroslav Ganin, Evgeniya Ustinova, Hana Ajakan, Pascal Germain, Hugo Larochelle, François Laviolette, Mario Marchand, and Victor S. Lempitsky. Domain-adversarial training of neural networks. *J. Mach. Learn. Res.*, 17:59:1–59:35, 2016.

[22] Ishaan Gulrajani and David Lopez-Paz. In search of lost domain generalization. In *ICLR*, 2021.

[23] Kaiming He, Xiangyu Zhang, Shaoqing Ren, and Jian Sun. Deep residual learning for image recognition. In *CVPR*, pages 770–778. IEEE, 2016.

[24] Dan Hendrycks and Thomas G. Dietterich. Benchmarking neural network robustness to common corruptions and perturbations. In *ICLR*, 2019.

[25] Dan Hendrycks and Kevin Gimpel. A baseline for detecting misclassified and out-of-distribution examples in neural networks. In *ICLR*, 2017.

[26] Evan Hernandez, Sarah Schwettmann, David Bau, Teona Bagashvili, Antonio Torralba, and Jacob Andreas. Natural language descriptions of deep visual features. In *ICLR*, 2022.

[27] Grant Van Horn, Oisin Mac Aodha, Yang Song, Yin Cui, Chen Sun, Alexander Shepard, Hartwig Adam, Pietro Perona, and Serge J. Belongie. The inaturalist species classification and detection dataset. In *CVPR*, pages 8769–8778. IEEE, 2018.

[28] Haiwen Huang, Zhihan Li, Lulu Wang, Sishuo Chen, Xinyu Zhou, and Bin Dong. Feature space singularity for out-of-distribution detection. In *SafeAI@AAAI*, 2021.

[29] Rui Huang, Andrew Geng, and Yixuan Li. On the importance of gradients for detecting distributional shifts in the wild. In *NeurIPS*, pages 677–689, 2021.

[30] Rui Huang and Yixuan Li. MOS: Towards scaling out-of-distribution detection for large semantic space. In *CVPR*, pages 8710–8719. IEEE, 2021.

[31] Dihong Jiang, Sun Sun, and Yaoliang Yu. Revisiting flow generative models for out-of-distribution detection. In *ICLR*, 2022.

[32] Daehee Kim, Youngjun Yoo, Seunghyun Park, Jinkyu Kim, and Jaekoo Lee. Selfreg: Self-supervised contrastive regularization for domain generalization. In *ICCV*, pages 9599–9608. IEEE, 2021.

[33] Polina Kirichenko, Pavel Izmailov, and Andrew Gordon Wilson. Why normalizing flows fail to detect out-of-distribution data. In *NeurIPS*, pages 20578–20589, 2020.

[34] Pang Wei Koh, Shiori Sagawa, Henrik Marklund, Sang Michael Xie, Marvin Zhang, Akshay Balsubramani, Weihua Hu, Michihiro Yasunaga, Richard Lanas Phillips, Irena Gao, Tony Lee, Etienne David, Ian Stavness, Wei Guo, Berton Earnshaw, Imran S. Haque, Sara M. Beery, Jure Leskovec, Anshul Kundaje, Emma Pierson, Sergey Levine, Chelsea Finn, and Percy Liang. WILDS: A benchmark of in-the-wild distribution shifts. In *ICML*, pages 5637–5664. PMLR, 2021.

[35] Alexander Kolesnikov, Lucas Beyer, Xiaohua Zhai, Joan Puigcerver, Jessica Yung, Sylvain Gelly, and Neil Houlsby. Big transfer (bit): General visual representation learning. In *ECCV*, pages 491–507. Springer, 2020.

[36] Steven G. Krantz. *Real Analysis and Foundations*. Chapman Hall/CRC, 2005.

[37] S. Kullback and R. A. Leibler. On Information and Sufficiency. *The Annals of Mathematical Statistics*, 22(1):79 – 86, 1951.

[38] Kimin Lee, Kibok Lee, Honglak Lee, and Jinwoo Shin. A simple unified framework for detecting out-of-distribution samples and adversarial attacks. In *NeurIPS*, pages 7167–7177, 2018.

[39] Da Li, Yongxin Yang, Yi-Zhe Song, and Timothy M. Hospedales. Deeper, broader and artier domain generalization. In *ICCV*, pages 5543–5551. IEEE, 2017.

[40] Da Li, Yongxin Yang, Yi-Zhe Song, and Timothy M. Hospedales. Learning to generalize: Meta-learning for domain generalization. In *AAAI*, pages 3490–3497. AAAI, 2018.

[41] Haoliang Li, Sinno Jialin Pan, Shiqi Wang, and Alex C. Kot. Domain generalization with adversarial feature learning. In *CVPR*, pages 5400–5409. IEEE, 2018.

[42] Shiyu Liang, Yixuan Li, and R. Srikant. Enhancing the reliability of out-of-distribution image detection in neural networks. In *ICLR*, 2018.

[43] Weitang Liu, Xiaoyun Wang, John D. Owens, and Yixuan Li. Energy-based out-of-distribution detection. In *NeurIPS*, pages 21464–21475, 2020.

[44] Lei Ma, Felix Juefei-Xu, Fuyuan Zhang, Jiyuan Sun, Minhui Xue, Bo Li, Chunyang Chen, Ting Su, Li Li, Yang Liu, Jianjun Zhao, and Yadong Wang. Deepgauge: multi-granularity testing criteria for deep learning systems. In *ASE*, pages 120–131. ACM, 2018.

[45] Yifei Ming, Yiyou Sun, Ousmane Dia, and Yixuan Li. How to exploit hyperspherical embeddings for out-of-distribution detection? In *ICLR*, 2023.

[46] Yuval Netzer, Tao Wang, Adam Coates, Alessandro Bissacco, Bo Wu, and Andrew Y. Ng. Reading digits in natural images with unsupervised feature learning. In *NeurIPS Workshop on Deep Learning and Unsupervised Feature Learning*, 2011.

[47] Giambattista Parascandolo, Alexander Neitz, Antonio Orvieto, Luigi Gresele, and Bernhard Schölkopf. Learning explanations that are hard to vary. In *ICLR*, 2021.

[48] Kexin Pei, Yinzhi Cao, Junfeng Yang, and Suman Jana. Deepxplore: Automated whitebox testing of deep learning systems. In *SOSP*, pages 1–18. ACM, 2017.

[49] Alexandre Ramé, Corentin Dancette, and Matthieu Cord. Fishr: Invariant gradient variances for out-of-distribution generalization. In *ICML*, pages 18347–18377. PMLR, 2022.

[50] Benjamin Recht, Rebecca Roelofs, Ludwig Schmidt, and Vaishaal Shankar. Do imagenet classifiers generalize to imagenet? In *ICML*, pages 5389–5400. PMLR, 2019.

[51] Shiori Sagawa, Pang Wei Koh, Tatsunori B. Hashimoto, and Percy Liang. Distributionally robust neural networks. In *ICLR*, 2020.

[52] Mark Sandler, Andrew G. Howard, Menglong Zhu, Andrey Zhmoginov, and Liang-Chieh Chen. Mobilenetv2: Inverted residuals and linear bottlenecks. In *CVPR*, pages 4510–4520. IEEE, 2018.

[53] Vikash Sehwag, Mung Chiang, and Prateek Mittal. SSD: A unified framework for self-supervised outlier detection. In *ICLR*, 2021.

[54] Lloyd S. Shapley. A value for n-person games. *Classics in game theory*, 69, 1997.

[55] Yuge Shi, Jeffrey Seely, Philip H. S. Torr, Siddharth Narayanaswamy, Awni Y. Hannun, Nicolas Usunier, and Gabriel Synnaeve. Gradient matching for domain generalization. In *ICLR*, 2022.

[56] Karen Simonyan and Andrew Zisserman. Very deep convolutional networks for large-scale image recognition. In *ICLR*, 2015.

[57] Baochen Sun and Kate Saenko. Deep CORAL: correlation alignment for deep domain adaptation. In *ECCV*, pages 443–450, 2016.

[58] Yiyou Sun, Chuan Guo, and Yixuan Li. React: Out-of-distribution detection with rectified activations. In *NeurIPS*, pages 144–157, 2021.

[59] Yiyou Sun and Yixuan Li. DICE: leveraging sparsification for out-of-distribution detection. In *ECCV*, pages 691–708. Springer, 2022.

[60] Yiyou Sun, Yifei Ming, Xiaojin Zhu, and Yixuan Li. Out-of-distribution detection with deep nearest neighbors. In *ICML*, pages 20827–20840. PMLR, 2022.

[61] Christian Szegedy, Wei Liu, Yangqing Jia, Pierre Sermanet, Scott E. Reed, Dragomir Anguelov, Dumitru Erhan, Vincent Vanhoucke, and Andrew Rabinovich. Going deeper with convolutions. In *CVPR*, pages 1–9. IEEE, 2015.

[62] Chris Xing Tian, Haoliang Li, Xiaofei Xie, Yang Liu, and Shiqi Wang. Neuron coverage-guided domain generalization. *IEEE Trans. Pattern Anal. Mach. Intell.*, 45(1):1302–1311, 2023.

[63] Joost van Amersfoort, Lewis Smith, Yee Whye Teh, and Yarin Gal. Uncertainty estimation using a single deep deterministic neural network. In *ICML*, pages 9690–9700. PMLR, 2020.

[64] Vladimir Vapnik. An overview of statistical learning theory. *IEEE Trans. Neural Networks*, 10(5):988–999, 1999.

[65] Hemanth Venkateswara, Jose Eusebio, Shayok Chakraborty, and Sethuraman Panchanathan. Deep hashing network for unsupervised domain adaptation. In *CVPR*, pages 5385–5394. IEEE, 2017.

[66] Jianxiong Xiao, James Hays, Krista A. Ehinger, Aude Oliva, and Antonio Torralba. SUN database: Large-scale scene recognition from abbey to zoo. In *CVPR*, pages 3485–3492. IEEE, 2010.

[67] Xiaofei Xie, Lei Ma, Felix Juefei-Xu, Minhui Xue, Hongxu Chen, Yang Liu, Jianjun Zhao, Bo Li, Jianxiong Yin, and Simon See. Deephunter: a coverage-guided fuzz testing framework for deep neural networks. In *ISSTA*, pages 146–157. ACM, 2019.

- [68] Pingmei Xu, Krista A. Ehinger, Yinda Zhang, Adam Finkelstein, Sanjeev R. Kulkarni, and Jianxiong Xiao. Turkergaze: Crowdsourcing saliency with webcam based eye tracking. *arXiv preprint arXiv:1504.06755*, 2015.
- [69] Xufeng Yao, Yang Bai, Xinyun Zhang, Yuechen Zhang, Qi Sun, Ran Chen, Ruiyu Li, and Bei Yu. Pcl: Proxy-based contrastive learning for domain generalization. In *CVPR*, pages 7097–7107. IEEE, 2022.
- [70] Fisher Yu, Yinda Zhang, Shuran Song, Ari Seff, and Jianxiong Xiao. LSUN: construction of a large-scale image dataset using deep learning with humans in the loop. *arXiv preprint arXiv:1506.03365*, 2015.
- [71] Yuanyuan Yuan, Qi Pang, and Shuai Wang. Revisiting neuron coverage for dnn testing: A layer-wise and distribution-aware criterion. In *ICSE*. ACM, 2023.
- [72] Bolei Zhou, Àgata Lapedriza, Aditya Khosla, Aude Oliva, and Antonio Torralba. Places: A 10 million image database for scene recognition. *IEEE Trans. Pattern Anal. Mach. Intell.*, 40(6):1452–1464, 2018.
- [73] Ev Zisselman and Aviv Tamar. Deep residual flow for out of distribution detection. In *CVPR*, pages 13991–14000. IEEE, 2020.

# Appendix

## Contents

---

<b>A</b>	<b>Potential Social Impact</b>	<b>15</b>
<b>B</b>	<b>Additional Theoretical Details</b>	<b>15</b>
<b>C</b>	<b>Approximation Details</b>	<b>16</b>
C.1	Preliminaries	16
C.2	Approximation	16
<b>D</b>	<b>Experimental Details for OOD Detection</b>	<b>17</b>
D.1	OOD Benchmarks	17
D.2	Model Architecture	17
D.3	Hyperparameters	18
<b>E</b>	<b>Experimental Details for OOD Generalization</b>	<b>18</b>
E.1	Domainbed Benchmark	18
E.2	Metric: Rank Correlation	19
E.3	Model Architecture	19
E.4	Hyperparameters	19
<b>F</b>	<b>Reproducibility</b>	<b>20</b>
F.1	Software and Hardware	20
F.2	Runtime Analysis	20
<b>G</b>	<b>Full Distribution Plots on ImageNet OOD benchmark</b>	<b>20</b>
<b>H</b>	<b>Full CIFAR Results</b>	<b>21</b>
<b>I</b>	<b>Full DomainBed Results</b>	<b>22</b>

---

## A Potential Social Impact

This study introduces neuron activation coverage (NAC) as an efficient tool for facilitating out-of-distribution (OOD) solutions. By improving OOD detection and generalization, NAC has the potential to significantly enhance the dependability and safety of modern machine learning models. Thus, the social impact of this research can be far-reaching, spanning consumer and business applications in digital content understanding, transportation systems including driver assistance and autonomous vehicles, as well as healthcare applications such as identifying unseen diseases. Moreover, by openly sharing our code, we strive to offer machine learning practitioners a readily available resource for responsible AI development, ultimately benefiting society as a whole. Although we anticipate no negative repercussions, we are committed to expanding upon our framework in future endeavors.

## B Additional Theoretical Details

Here, we present additional theoretical details for Eq. (3) in the main paper. Specifically, we elaborate on the calculation of gradients *w.r.t.* the sample confidence. As a reminder, in the main paper, we introduce the Kullback-Leibler (KL) divergence [37] between the network output and a uniform vector  $\mathbf{u} = [1/C, 1/C, \dots, 1/C] \in \mathbb{R}^C$  as follows:

$$\begin{aligned} D_{\text{KL}}(\mathbf{u} \parallel \mathbf{p}) &= \sum_{i=1}^C u_i \log \frac{u_i}{p_i} \\ &= - \sum_{i=1}^C u_i \log p_i + \sum_{i=1}^C u_i \log u_i \\ &= -\frac{1}{C} \sum_{i=1}^C \log p_i - H(\mathbf{u}), \end{aligned}$$

where  $\mathbf{p} = \text{softmax}(F(\mathbf{x}))$ , and  $p_i$  denotes  $i$ -element in  $\mathbf{p}$ .  $H(\mathbf{u}) = -\sum_{i=1}^C u_i \log u_i$  is a constant. Let  $F(\mathbf{x})_i$  indicates  $i$ -th element in  $F(\mathbf{x})$ , we have  $p_i = e^{F(\mathbf{x})_i} / \sum_{j=1}^C e^{F(\mathbf{x})_j}$ . Then, by substituting the expression of  $p_i$ , we can rewrite KL divergence as:

$$\begin{aligned} D_{\text{KL}}(\mathbf{u} \parallel \text{softmax}(F(\mathbf{x}))) &= -\frac{1}{C} \sum_{i=1}^C \log \frac{e^{F(\mathbf{x})_i}}{\sum_{j=1}^C e^{F(\mathbf{x})_j}} - H(\mathbf{u}) \\ &= -\frac{1}{C} \left( \sum_{i=1}^C F(\mathbf{x})_i - C \cdot \log \sum_{j=1}^C e^{F(\mathbf{x})_j} \right) - H(\mathbf{u}). \end{aligned}$$

Subsequently, we can drive the gradients of KL divergence *w.r.t.* the output logit  $F(\mathbf{x})_i$  as:

$$\begin{aligned} \frac{\partial D_{\text{KL}}}{\partial F(\mathbf{x})_i} &= -\frac{1}{C} \left( 1 - C \cdot \frac{\partial \log \sum_{j=1}^C e^{F(\mathbf{x})_j}}{\partial F(\mathbf{x})_i} \right) \\ &= -\frac{1}{C} \left( 1 - C \cdot \frac{e^{F(\mathbf{x})_i}}{\sum_{j=1}^C e^{F(\mathbf{x})_j}} \right) \\ &= -\frac{1}{C} + \frac{e^{F(\mathbf{x})_i}}{\sum_{j=1}^C e^{F(\mathbf{x})_j}} \\ &= p_i - u_i. \end{aligned}$$

Since  $F(\mathbf{x}) = g(f(\mathbf{x})) = g(\mathbf{z})$ , we finally have:

$$\frac{\partial D_{\text{KL}}}{\partial g(\mathbf{z})} = \frac{\partial D_{\text{KL}}}{\partial F(\mathbf{x})} = [p_1 - u_1, \dots, p_c - u_c]^T = \mathbf{p} - \mathbf{u} \quad (9)$$

## C Approximation Details

In this section, we demonstrate details for the approximation of PDF, and further show the insights for the choice of  $r$  in our NAC function.

### C.1 Preliminaries

**Probability density function (PDF).** The Probability Density Function (PDF), denoted by  $\kappa(x)$ , measures the probability of a continuous random variable taking on a specific value within a given range. Accordingly,  $\kappa(x)$  should possess the following key properties:

- (1) Non-Negativity:  $\kappa(x) \geq 0$ , for all  $x \in \mathbb{R}$ ;
- (2) Normalization:  $\int_{-\infty}^{\infty} \kappa(x)dx = 1$ ;
- (3) Probability Interpretation:  $P(a \leq \mu \leq b) = \int_a^b \kappa(x)dx$ ,

where  $P(a \leq \mu \leq b)$  denotes the probability that random variable  $\mu$  has values within range  $[a, b]$ .

**Cumulative distribution function (CDF).** In line with PDF, the Cumulative Distribution Function (CDF), denoted by  $K(x)$ , calculates the cumulative probability for a given  $x$ -value. Formally,  $K(x)$  gives the area under the probability density function up to the specified  $x$ ,

$$K(x) = P(\mu \leq x) = \int_{-\infty}^x \kappa(t)dt. \quad (10)$$

By the Fundamental Theorem of Calculus, we can rewrite the function  $\kappa(x)$  as,

$$\kappa(x) = K'(x) = \lim_{h \rightarrow 0} \frac{K(x+h) - K(x)}{h}. \quad (11)$$

Note that in the main paper, we denote by  $\kappa_X^i(\cdot)$  the PDF, and  $\Phi_X^i(\cdot)$  the NAC function of  $i$ -th neuron over the dataset  $X$ . In this appendix, we will omit the superscript  $i$  and subscript  $X$  for simplicity.

### C.2 Approximation

In accordance with the main paper, the approximation of PDF follows the typical histogram-based approach. Specifically, since the length of neuron activation space is 1 (bounded by the sigmoid function), we approximate PDF function by partitioning the neuron activation space into  $M$  equally-spaced intervals/bins (each bin has a width  $h = 1/M$ ), such that

$$\kappa(\hat{z}) \approx \frac{K(\hat{z} + h) - K(\hat{z})}{h} = \frac{P(\hat{z} < \mu \leq \hat{z} + h)}{h} \approx \frac{O(\hat{z})}{|X|} \cdot \frac{1}{h}, \quad (12)$$

where  $\hat{z}$  is the neuron activation state, and  $O(\hat{z})$  is the number of samples in the bin containing  $\hat{z}$ .

**The choice of  $r$ .** With the approximation of PDF, we can rewrite the NAC function as,

$$\Phi(\hat{z}; r) = \frac{1}{r} \min(\kappa(\hat{z}), r) = \min\left(\frac{\kappa(\hat{z})}{r}, 1\right) \approx \min\left(\frac{O(\hat{z})}{|X|h} \cdot \frac{1}{r}, 1\right), \quad (13)$$

where  $r$  denotes the lower bound for achieving full coverage *w.r.t.* state  $\hat{z}$ . However, for the above formulation, it could be challenging to search for a suitable  $r$ , since various factors (*e.g.*, InD dataset size  $|X|$ ) could affect the significance of NAC scores  $\Phi(\hat{z}; r)$ . In this sense, to further simplify this formulation in the practical deployment, we set  $r = \frac{O^*}{|X|h}$ , such that

$$\Phi(\hat{z}; r) \approx \min\left(\frac{O(\hat{z})}{|X|h} \cdot \frac{1}{r}, 1\right) = \min\left(\frac{O(\hat{z})}{O^*}, 1\right), \quad (14)$$

where  $O^*$  represents the minimum number of samples required to fill a bin completely, and  $O(\hat{z})$  is the number of samples in the bin containing  $\hat{z}$ . In this way, we can directly manipulate  $O^*$  to control the NAC function in the practical deployment.

## D Experimental Details for OOD Detection

### D.1 OOD Benchmarks

We conduct experiments following previous SoTA approaches [58, 29, 18, 2, 30, 43]. Here we provide more details for the utilized two benchmarks: ImageNet and CIFAR benchmark.

**Large-scale ImageNet benchmark** We employ ImageNet-1k [16] as the in-distribution dataset, and conduct evaluations on four out-of-distribution (OOD) test datasets, following the specified setup [30]:

1. **iNaturalist** [27]: This dataset consists of 859,000 images of plants and animals, covering over 5,000 different species. Each image is resized to a maximum dimension of 800 pixels. Following [30], we evaluate our method on a randomly selected subset of 10,000 images, which are drawn from 110 classes that do not overlap with ImageNet-1k.
2. **SUN** [66]: With over 130,000 images, SUN includes scenes from 397 categories. Since there are some categories overlapping with ImageNet-1k, we randomly sample 10,000 images from 50 classes that are distinct from ImageNet labels for evaluation.
3. **Places** [72]: Similar to SUN, Places is another scene dataset encompassing comparable conceptual categories. We select a subset of 10,000 images across 50 classes that are not included in ImageNet-1k for evaluation.
4. **Textures** [14]: This dataset contains 5,640 real-world texture images categorized into 47 classes. We utilize the entire dataset for evaluation purposes.

**CIFAR benchmark** CIFAR-10 and CIFAR-100 are widely employed as in-distribution (ID) datasets in current studies. CIFAR-10 consists of 10 classes, while CIFAR-100 contains 100 classes. We follow the standard split, utilizing 50,000 training images and 10,000 test images. Following [18, 58, 59], to assess the performance of our approach, we conduct evaluations on six commonly used out-of-distribution (OOD) datasets, which are detailed below:

1. **SVHN** [46]: This dataset consists of color images depicting house numbers, encompassing ten classes representing digits 0 to 9. We utilize the entire test set, containing 26,032 images.
2. **LSUN-Crop** [70]: This dataset builds upon the LSUN dataset, containing 10,000 test images distributed across ten different scenes. For this LSUN-Crop, we randomly crop LSUN image patches of size 32x32.
3. **LSUN-Resize** [70]: Likewise, LSUN-Resize is produced by downsampling each LSUN image to the size 32x32.
4. **iSUN** [68]: This dataset comprises the ground truth of gaze traces on images from the SUN dataset. We employ the entire dataset for evaluation, which contains 8,925 images.
5. **Places365** [72]: Places365 contains a vast collection of photographs depicting scenes, classified into 365 scene categories. The test set consists of 900 images per category. For evaluation, we utilize the entire test dataset containing 328,500 images following [58].
6. **Textures** [14]: The Textures dataset comprises 5,640 real-world texture images classified into 47 categories. We employ the entire dataset for evaluation purposes.

### D.2 Model Architecture

In summary, our experiments for ImageNet benchmark employ three model architectures:

- ResNet-50 [23] is pretrained on ImageNet-1k. For this model, all images are resized to  $224 \times 224$  at the test phase.
- BiTS-R101x1 [35] is pre-trained on ImageNet-1k with a ResNetv2-101 [23] architecture <sup>2</sup>. At test time, all images are resized to  $480 \times 480$  for this model.
- MobileNet-v2 [52] is also pretrained on ImageNet-1k. Similar to ResNet-50, all images are resized to  $224 \times 224$  at the test phase.

<sup>2</sup> [https://github.com/google-research/big\\_transfer](https://github.com/google-research/big_transfer)

For CIFAR benchmarks, we employ the powerful ResNet-18 [23] architecture. In line with the ReAct [58], we train a ResNet-18 model using standard in-distribution data. We train the models for 100 epochs for both CIFAR-10 and CIFAR-100 datasets. The initial learning rate is set to 0.1 and is reduced by a factor of 10 at epochs 50, 75, and 90.

### D.3 Hyperparameters

In Table 9 and Table 10, we list the values of hyperparameters for different model architectures over ImageNet and CIFAR benchmarks. In our experiments, we find that improving the number of intervals, and choosing deeper layers are beneficial for the final results.

Architecture	Parameter	Denotation	Value
ResNet-50	-	layer choice	Layer4
	$M$	number of intervals for PDF approximation	10000
	$\alpha$	sigmoid steepness	1000
	$r$	lower bound for full coverage	1.0
	$O^*$	minimum number of samples to fill a bin	5
BiTS-R101x1	-	layer choice	Block4
	$M$	number of intervals for PDF approximation	10000
	$\alpha$	sigmoid steepness	1000
	$r$	lower bound for full coverage	1.0
	$O^*$	minimum number of samples to fill a bin	5
MobileNet-v2	-	layer choice	Layer18
	$M$	number of intervals for PDF approximation	30000
	$\alpha$	sigmoid steepness	1000
	$r$	lower bound for full coverage	0.6
	$O^*$	minimum number of samples to fill a bin	1

Table 9: Hyperparameters and their default values on ImageNet benchmark. Note that  $r$  is computed based on  $O^*$ , as illustrated in Appendix C.2

Architecture	Parameter	Denotation	Value
ResNet-18	-	layer choice	Layer4
	$M$	number of intervals for PDF approximation	10000
	$\alpha$	sigmoid steepness	1000
	$r$	lower bound for full coverage	1.0
	$O^*$	minimum number of samples to fill a bin	1

Table 10: Hyperparameters and their default values on CIFAR-10 and CIFAR-100 benchmarks. Note that  $r$  is computed based on  $O^*$ , as illustrated in Appendix C.2

## E Experimental Details for OOD Generalization

### E.1 Domainbed Benchmark

**Datasets** We conduct experiments on DomainBed [22] benchmark, which is an arguably fairer benchmark in OOD generalization<sup>3</sup>. Without utilizing digital images, we utilize four datasets:

1. VLCS [20] is composed of photographic domains, namely Caltech101, LabelMe, SUN09, and VOC2007. This dataset consists of 10,729 examples with dimensions (3, 224, 224) and 5 classes.
2. PACS dataset [39] consists of four domains: `art`, `cartoons`, `photos`, and `sketches`. It comprises a total of 9,991 examples with dimensions (3, 224, 224) and 7 classes.
3. OfficeHome [65] includes domains: `art`, `clipart`, `product`, `real`. This dataset contains 15,588 examples of dimension (3, 224, 224) and 65 classes.

<sup>3</sup><https://github.com/facebookresearch/DomainBed>.

4. TerraInc [7] is a collection of wildlife photographs captured by camera traps at various locations: L100, L38, L43, and L46. Our version of this dataset contains 24,788 examples of dimension (3, 224, 224) and 10 classes.

**Settings** To ensure the reliability of final results, the data from each domain is partitioned into two parts: 80% for training or testing, and 20% for validation. This process is repeated three times with different seeds, such that reported numbers represent the mean and standard errors across these three runs. In our experiments, we report *leave-one-out* test accuracy scores, whereby results are averaged over cases that use a single domain for test and the others for training. Besides, we set the total training steps as 5000, and the evaluation frequency as 300 steps for all runs.

**Model evaluation criteria** For model evaluation, we mainly compare our method with the *validation criterion*, which measures model accuracy over 20% source-domain validation data. In addition, we also employ the *oracle criterion* as the upper bound, which directly utilizes the accuracy over 20% test-domain data for model evaluation. For more details, we suggest to refer [22].

## E.2 Metric: Rank Correlation

Rank correlation metrics are widely utilized to measure the extent to which an increase in the value of one random variable aligns with an increase in the another random variable. Following [5], we utilize the Spearman Rank Correlation (RC) for assessing the relationship between OOD test accuracy and the model evaluation scores (*i.e.*, InD validation accuracy or InD NAC scores).

The rationale behind this choice is that during the training phase, the selection of the optimal model is frequently based on ranking the model performance, such as validation accuracy. Therefore, utilizing the RC score enables us to directly measure the effectiveness of evaluation criteria in model selection (which naturally translates to early stopping). The value of RC ranges between -1 and 1, where a value of -1 signifies that the rankings of two random variables are exactly opposite to each other; whereas, a value of +1 indicates that the rankings are exactly the same. Furthermore, a RC score of 0 indicates no linear relationship between the two variables.

## E.3 Model Architecture

In our experiments, we employ four model architectures: ResNet-18 [23], ResNet-50 [23], Vit-t16 [19], and Vit-b16 [19]. All of them are pretrained on the ImageNet dataset, and are employed as the initial weight. We utilize the Adam optimizer to optimize initialized models and set the learning rate of 5e-5. For other parameter choices, we suggest to refer [10].

## E.4 Hyperparameters

In the case of ResNet architectures, NAC computation is performed using the neurons in *Layer-4*. For ResNet-50, Layer-4 consists of 2048 neurons, while ResNet-18 has 512 neurons. As for vision transformers, NAC computation utilizes the neurons in *MLP-11*. In Vit-b16, MLP-11 comprises 3072 neurons; whereas Vit-t16 has 768 neurons. During this series of experiments, we employ the source-domain training data to formulate the NAC function. To mitigate noises in training samples, we merely utilize training data that can be correctly classified, to formulate the NAC function.

In order to determine the hyperparameters for all models, we employ a random search method based on the parameter distribution outlined in Table 11. This random search approach can be seamlessly integrated with the DomainBed parameter-search table, thereby facilitating model adaptation.

Parameter	Denotation	Random distribution
$M$	number of intervals for PDF approximation	10000
$\alpha$	sigmoid steepness	RandomChoice([1, 10, 100, 1000])
$O^*$	minimum number of samples to fill a bin	RandomChoice([1, 5, 10, 100, 1000, 5000])

Table 11: Hyperparameters of our NAC-ME and their distributions for random search. Note that  $r$  can be computed based on  $O^*$ , as illustrated in Appendix C.2

## F Reproducibility

We will publicly release our code with detailed instructions.

### F.1 Software and Hardware

All experiments are performed on a single NVIDIA GeForce RTX 3090 GPU, with Python version 3.8.11. The deep learning framework used is PyTorch 1.10.0, and Torchvision version 0.11.1 is utilized for image processing. We leverage CUDA 11.3 for GPU acceleration.

### F.2 Runtime Analysis

The total runtime of the experiments varies depending on the tasks and datasets. In the following, we provide details for two OOD tasks with resent50 architecture, using a single NVIDIA GeForce RTX 3090 GPU. For OOD detection, the experiments (*e.g.*, inference during the test phase) take approximately 10 minutes for all benchmarks. For OOD generalization, the experiments on average take approximately 4 hours for PACS and VLCS, 8 hours for OfficeHome, 8.5 hours for TerraInc.

## G Full Distribution Plots on ImageNet OOD benchmark

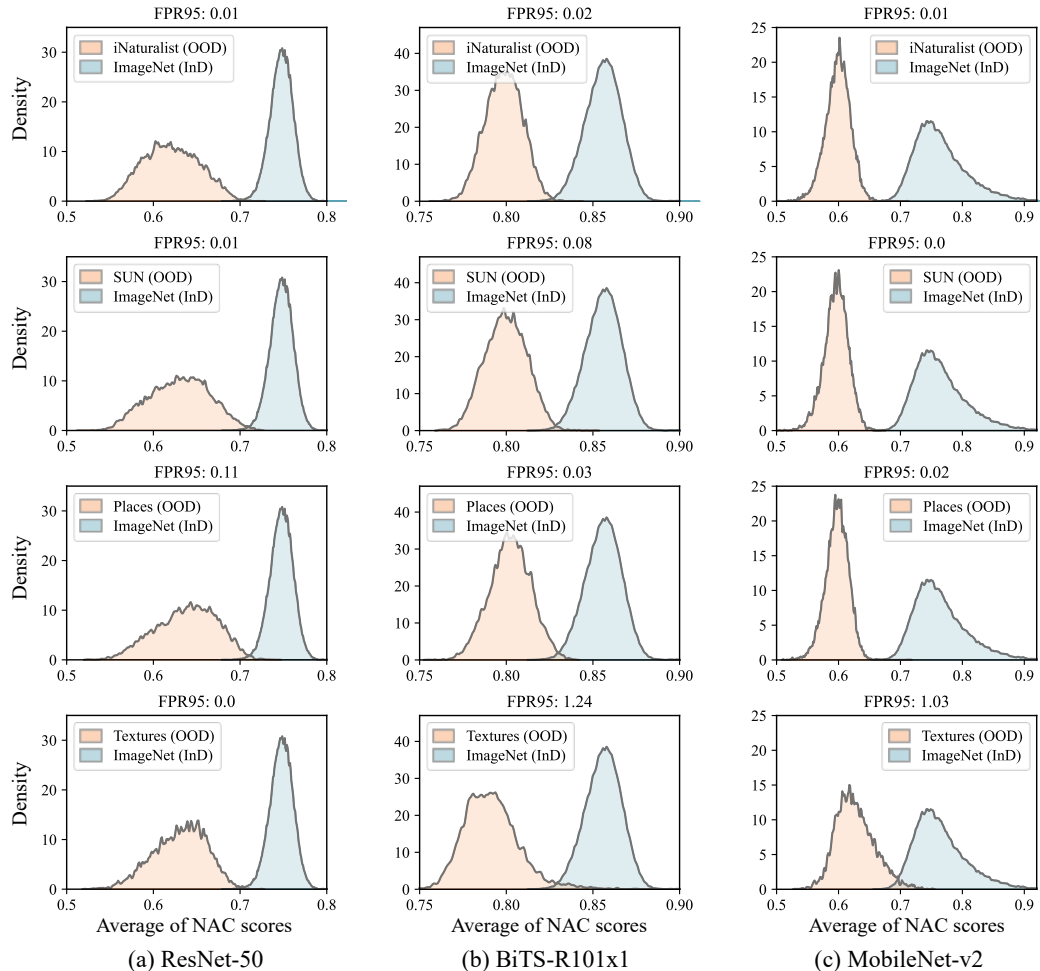


Figure 6: Distribution of uncertainty scores *w.r.t.* our NAC-UE. We visualize the results over three backbones, which are solely trained on ImageNet-1k.

## H Full CIFAR Results

Method	SVHN [46]			LSUN-Crop [70]			LSUN-Resize [70]			iSUN [68]			Textures [14]			Places365 [72]			Average		
	FPR95 ↓	AUROC ↑	FPR95 ↓	AUROC ↑	FPR95 ↓	AUROC ↑	FPR95 ↓	AUROC ↑	FPR95 ↓	AUROC ↑	FPR95 ↓	AUROC ↑	FPR95 ↓	AUROC ↑	FPR95 ↓	AUROC ↑	FPR95 ↓	AUROC ↑	FPR95 ↓	AUROC ↑	
<i>OOD Benchmark: CIFAR-10</i>																					
MSP [25]	59.66	91.25	45.21	93.80	51.93	92.73	54.57	92.12	66.45	88.5	62.46	88.64	56.71	91.17							
ODIN [42]	60.37	88.27	7.81	98.58	9.24	98.25	11.62	97.91	52.09	89.17	45.49	90.58	31.10	93.79							
Energy [43]	54.41	91.22	10.19	98.05	23.45	96.14	27.52	95.59	55.23	89.37	42.77	91.02	35.60	93.57							
ReAct [58]	49.77	92.18	16.99	97.11	17.94	96.98	20.84	96.46	47.96	91.55	43.97	91.33	32.91	94.27							
<b>NAC-UE (Ours)</b>	<b>0.08</b> <sub>±0.00</sub>	<b>99.97</b> <sub>±0.00</sub>	<b>0.02</b> <sub>±0.03</sub>	<b>100.00</b> <sub>±0.01</sub>	<b>0.02</b> <sub>±0.11</sub>	<b>99.99</b> <sub>±0.03</sub>	<b>0.17</b> <sub>±0.34</sub>	<b>99.96</b> <sub>±0.07</sub>	<b>0.66</b> <sub>±0.07</sub>	<b>99.96</b> <sub>±0.00</sub>	<b>0.91</b> <sub>±0.00</sub>	<b>100.00</b> <sub>±0.00</sub>	<b>0.00</b> <sub>±0.00</sub>	<b>100.00</b> <sub>±0.00</sub>	<b>0.16</b>	<b>99.95</b>					
<i>OOD Benchmark: CIFAR-100</i>																					
MSP [25]	81.32	77.74	70.11	83.51	82.46	75.73	82.26	76.16	85.11	73.36	83.06	74.47	80.72	76.83							
ODIN [42]	40.94	93.29	28.72	94.51	79.61	82.13	76.66	83.51	83.63	72.37	87.71	71.46	66.21	82.88							
Energy [43]	81.74	84.56	34.78	93.93	73.57	82.99	73.36	83.80	85.87	74.94	82.23	76.68	71.93	82.82							
ReAct [58]	70.81	88.24	39.99	92.51	54.47	89.56	51.89	90.12	59.15	87.96	81.33	76.49	59.61	87.48							
<b>NAC-UE (Ours)</b>	<b>0.01</b> <sub>±0.00</sub>	<b>99.97</b> <sub>±0.01</sub>	<b>0.00</b> <sub>±0.01</sub>	<b>99.98</b> <sub>±0.01</sub>	<b>0.00</b> <sub>±0.00</sub>	<b>99.99</b> <sub>±0.01</sub>	<b>0.00</b> <sub>±0.00</sub>	<b>99.99</b> <sub>±0.02</sub>	<b>0.00</b> <sub>±0.00</sub>	<b>99.74</b> <sub>±0.02</sub>	<b>0.00</b> <sub>±0.01</sub>	<b>1.19</b> <sub>±0.20</sub>	<b>0.20</b>	<b>99.94</b>							

Table 12: OOD detection results on CIFAR-10 and CIFAR-100. We report the performance over ResNet-18 backbone, which is trained solely on the Ind dataset, *i.e.*, CIFAR.  $\uparrow$  denotes the higher value is better, while  $\downarrow$  indicates lower values are better. The results of our methods are averaged over 20 random seeds.

## I Full DomainBed Results

Method	Caltech101		LabelMe		SUN09		VOC2007		Average		
	RC	ACC	RC	ACC	RC	ACC	RC	ACC	RC	ACC	
RN18	Oracle	-	96.00 $\pm$ 0.8	-	65.10 $\pm$ 0.3	-	71.34 $\pm$ 0.8	-	76.24 $\pm$ 0.4	-	
	Validation	36.03 $\pm$ 17.3	95.38 $\pm$ 0.9	17.57 $\pm$ 13.2	63.62 $\pm$ 1.1	50.33 $\pm$ 13.6	67.73 $\pm$ 0.6	33.17 $\pm$ 15.7	73.75 $\pm$ 0.7	34.27	75.12
	NAC-ME	71.41 $\pm$ 2.6	96.17 $\pm$ 0.7	5.64 $\pm$ 1.0	61.54 $\pm$ 1.3	65.28 $\pm$ 8.3	71.44 $\pm$ 0.8	65.69 $\pm$ 10.4	75.23 $\pm$ 0.5	52.00	76.10
RN50	Oracle	-	98.47 $\pm$ 0.3	-	68.69 $\pm$ 0.8	-	73.46 $\pm$ 0.9	-	78.07 $\pm$ 0.3	-	
	Validation	20.75 $\pm$ 17.0	98.00 $\pm$ 0.2	35.29 $\pm$ 13.2	65.16 $\pm$ 1.4	33.01 $\pm$ 3.1	70.37 $\pm$ 0.6	36.68 $\pm$ 4.3	77.28 $\pm$ 0.3	31.43	77.70
	NAC-ME	57.92 $\pm$ 2.5	98.50 $\pm$ 0.3	-4.74 $\pm$ 3.9	60.27 $\pm$ 0.6	35.54 $\pm$ 13.2	70.88 $\pm$ 2.1	26.39 $\pm$ 7.2	77.13 $\pm$ 0.8	28.78	76.69
ViT-16	Oracle	-	97.91 $\pm$ 0.3	-	66.67 $\pm$ 0.3	-	73.47 $\pm$ 0.9	-	75.54 $\pm$ 0.1	-	
	Validation	30.72 $\pm$ 2.0	98.35 $\pm$ 0.2	45.92 $\pm$ 3.3	63.91 $\pm$ 0.6	50.65 $\pm$ 4.6	72.62 $\pm$ 0.3	35.21 $\pm$ 10.6	75.31 $\pm$ 0.7	40.63	77.55
	NAC-ME	55.47 $\pm$ 1.5	98.47 $\pm$ 0.1	9.80 $\pm$ 1.6	63.75 $\pm$ 0.4	72.96 $\pm$ 6.6	74.02 $\pm$ 0.2	42.81 $\pm$ 4.1	74.48 $\pm$ 0.2	45.26	77.68
ViT-b16	Oracle	-	97.70 $\pm$ 0.6	-	66.29 $\pm$ 0.5	-	78.26 $\pm$ 0.4	-	79.50 $\pm$ 0.9	-	
	Validation	-11.27 $\pm$ 10.8	96.85 $\pm$ 0.7	51.80 $\pm$ 5.0	64.39 $\pm$ 1.0	28.76 $\pm$ 10.2	76.24 $\pm$ 1.1	50.49 $\pm$ 16.1	79.08 $\pm$ 0.6	29.94	79.14
	NAC-ME	64.22 $\pm$ 6.1	98.23 $\pm$ 0.2	16.99 $\pm$ 4.2	63.69 $\pm$ 0.6	19.36 $\pm$ 9.2	76.15 $\pm$ 0.3	34.48 $\pm$ 9.3	78.13 $\pm$ 0.7	33.76	79.05

Table 13: OOD generalization results on VLCS dataset [20]. *Oracle* indicates the upper bound. The training strategy is ERM [64]. All scores are averaged over 3 random trials.

Method	Art		Cartoon		Photo		Sketch		Average		
	RC	ACC	RC	ACC	RC	ACC	RC	ACC	RC	ACC	
RN18	Oracle	-	78.48 $\pm$ 0.1	-	75.05 $\pm$ 0.8	-	94.26 $\pm$ 0.4	-	72.74 $\pm$ 1.5	-	
	Validation	72.22 $\pm$ 5.1	77.32 $\pm$ 0.7	65.20 $\pm$ 6.6	71.91 $\pm$ 0.7	60.87 $\pm$ 7.1	94.44 $\pm$ 0.2	76.55 $\pm$ 1.2	72.36 $\pm$ 1.1	68.71	79.01
	NAC-ME	71.32 $\pm$ 5.5	77.93 $\pm$ 0.4	75.16 $\pm$ 2.7	71.54 $\pm$ 0.8	60.62 $\pm$ 6.6	94.64 $\pm$ 0.2	83.09 $\pm$ 1.5	72.37 $\pm$ 1.3	72.55	79.12
RN50	Oracle	-	86.11 $\pm$ 0.5	-	80.99 $\pm$ 0.4	-	97.73 $\pm$ 0.2	-	76.82 $\pm$ 1.1	-	
	Validation	70.26 $\pm$ 9.1	86.72 $\pm$ 0.5	65.93 $\pm$ 10.3	78.86 $\pm$ 1.3	38.73 $\pm$ 12.3	97.83 $\pm$ 0.1	59.23 $\pm$ 11.4	74.87 $\pm$ 1.1	58.54	84.57
	NAC-ME	72.88 $\pm$ 1.5	86.72 $\pm$ 0.5	75.57 $\pm$ 4.5	78.48 $\pm$ 1.4	29.25 $\pm$ 16.0	97.68 $\pm$ 0.1	68.38 $\pm$ 8.8	76.66 $\pm$ 1.2	61.52	84.89
ViT-16	Oracle	-	75.68 $\pm$ 0.2	-	66.01 $\pm$ 0.7	-	96.26 $\pm$ 0.2	-	49.36 $\pm$ 1.8	-	
	Validation	88.40 $\pm$ 4.3	75.59 $\pm$ 0.2	92.73 $\pm$ 1.7	65.41 $\pm$ 0.4	91.58 $\pm$ 2.5	96.13 $\pm$ 0.2	80.96 $\pm$ 4.7	41.95 $\pm$ 2.2	88.42	69.77
	NAC-ME	87.42 $\pm$ 4.3	75.59 $\pm$ 0.2	93.71 $\pm$ 0.9	64.09 $\pm$ 0.6	91.75 $\pm$ 2.0	96.13 $\pm$ 0.2	87.99 $\pm$ 2.2	48.76 $\pm$ 1.7	90.22	71.14
ViT-b16	Oracle	-	94.79 $\pm$ 0.2	-	83.99 $\pm$ 0.5	-	99.55 $\pm$ 0.1	-	78.06 $\pm$ 0.6	-	
	Validation	9.56 $\pm$ 5.2	93.37 $\pm$ 0.6	41.50 $\pm$ 8.0	82.36 $\pm$ 0.4	45.67 $\pm$ 6.0	99.65 $\pm$ 0.1	29.41 $\pm$ 10.8	72.07 $\pm$ 3.3	31.54	86.86
	NAC-ME	29.74 $\pm$ 3.1	93.27 $\pm$ 0.6	53.02 $\pm$ 4.4	83.92 $\pm$ 0.1	38.97 $\pm$ 16.5	99.40 $\pm$ 0.2	39.46 $\pm$ 14.8	76.19 $\pm$ 2.0	40.30	88.19

Table 14: OOD generalization results on PACS dataset [39]. *Oracle* indicates the upper bound. The training strategy is ERM [64]. All scores are averaged over 3 random trials.

Method	Art		Clipart		Product		Real		Average	
	RC	ACC	RC	ACC	RC	ACC	RC	ACC	RC	ACC
RN18	Oracle	-	47.99 $\pm$ 0.2	-	41.99 $\pm$ 0.2	-	66.22 $\pm$ 0.1	-	67.79 $\pm$ 0.4	-
	Validation	<b>86.36<math>\pm</math>1.9</b>	<b>47.68<math>\pm</math>0.3</b>	75.33 $\pm$ 3.2	41.16 $\pm$ 0.6	88.73 $\pm$ 3.3	65.82 $\pm$ 0.1	83.58 $\pm$ 3.1	67.73 $\pm$ 0.4	83.50
	NAC-ME	86.19 $\pm$ 2.5	<b>47.68<math>\pm</math>0.1</b>	<b>77.61<math>\pm</math>5.7</b>	<b>41.26<math>\pm</math>0.6</b>	<b>91.09<math>\pm</math>1.8</b>	<b>66.10<math>\pm</math>0.1</b>	<b>84.23<math>\pm</math>5.0</b>	<b>68.16<math>\pm</math>0.1</b>	<b>84.78</b>
RN50	Oracle	-	59.46 $\pm$ 0.6	-	50.29 $\pm$ 0.5	-	75.08 $\pm$ 0.2	-	75.75 $\pm$ 0.2	-
	Validation	71.32 $\pm$ 4.2	59.01 $\pm$ 0.5	53.43 $\pm$ 6.5	<b>50.29<math>\pm</math>0.4</b>	<b>81.21<math>\pm</math>5.7</b>	<b>74.96<math>\pm</math>0.5</b>	<b>65.77<math>\pm</math>7.0</b>	<b>75.88<math>\pm</math>0.2</b>	67.93
	NAC-ME	<b>79.00<math>\pm</math>7.4</b>	<b>59.87<math>\pm</math>0.4</b>	<b>59.15<math>\pm</math>3.1</b>	50.19 $\pm$ 0.4	78.68 $\pm$ 5.3	74.66 $\pm$ 0.4	60.13 $\pm$ 7.3	75.86 $\pm$ 0.1	<b>69.24</b>
ViT-b16	Oracle	-	56.85 $\pm$ 0.2	-	43.38 $\pm$ 0.4	-	71.83 $\pm$ 0.1	-	72.92 $\pm$ 0.1	-
	Validation	<b>98.77<math>\pm</math>0.4</b>	<b>56.27<math>\pm</math>0.3</b>	97.79 $\pm$ 0.5	43.35 $\pm$ 0.5	98.45 $\pm$ 0.5	<b>71.64<math>\pm</math>0.2</b>	98.86 $\pm$ 0.3	<b>73.12<math>\pm</math>0.1</b>	98.47
	NAC-ME	98.04 $\pm$ 0.3	55.89 $\pm$ 0.2	<b>98.94<math>\pm</math>0.4</b>	<b>43.43<math>\pm</math>0.5</b>	<b>98.86<math>\pm</math>0.4</b>	71.43 $\pm$ 0.1	<b>99.43<math>\pm</math>0.2</b>	<b>73.12<math>\pm</math>0.1</b>	<b>98.82</b>
ViT-b16	Oracle	-	74.51 $\pm$ 6.6	-	71.73 $\pm$ 10.3	-	68.63 $\pm$ 8.9	-	47.06 $\pm$ 6.5	-
	Validation	<b>78.59<math>\pm</math>4.4</b>	78.32 $\pm$ 0.3	52.94 $\pm$ 5.4	<b>66.72<math>\pm</math>0.3</b>	59.15 $\pm$ 6.0	87.46 $\pm$ 0.1	<b>70.26<math>\pm</math>2.9</b>	89.30 $\pm$ 0.2	65.24
	NAC-ME	75.41 $\pm$ 2.8	<b>78.90<math>\pm</math>0.3</b>	<b>64.46<math>\pm</math>6.7</b>	66.62 $\pm$ 0.1	<b>66.01<math>\pm</math>6.4</b>	<b>87.61<math>\pm</math>0.1</b>	67.65 $\pm$ 8.3	<b>89.48<math>\pm</math>0.2</b>	<b>68.38</b>

Table 15: OOD generalization results on OfficeHome dataset [65]. *Oracle* indicates the upper bound. The training strategy is ERM [64]. All scores are averaged over 3 random trials.

Method	Loc100		Loc38		Loc43		Loc46		Average	
	RC	ACC	RC	ACC	RC	ACC	RC	ACC	RC	ACC
RN18	Oracle	-	54.82 $\pm$ 1.3	-	36.20 $\pm$ 0.2	-	51.75 $\pm$ 0.3	-	34.51 $\pm$ 0.7	-
	Validation	13.48 $\pm$ 12.5	45.20 $\pm$ 0.3	46.32 $\pm$ 10.9	<b>29.90<math>\pm</math>2.6</b>	55.15 $\pm$ 13.8	47.69 $\pm$ 1.2	40.11 $\pm$ 2.7	<b>33.35<math>\pm</math>0.1</b>	38.77
	NAC-ME	<b>13.81<math>\pm</math>12.8</b>	<b>48.25<math>\pm</math>2.3</b>	<b>46.81<math>\pm</math>11.1</b>	29.59 $\pm$ 2.7	<b>55.72<math>\pm</math>13.2</b>	<b>51.02<math>\pm</math>0.3</b>	<b>40.77<math>\pm</math>0.8</b>	32.79 $\pm$ 0.4	<b>39.28</b>
RN50	Oracle	-	55.62 $\pm$ 0.5	-	45.12 $\pm$ 1.1	-	56.92 $\pm$ 0.3	-	43.26 $\pm$ 0.9	-
	Validation	43.95 $\pm$ 7.6	49.08 $\pm$ 3.5	<b>36.60<math>\pm</math>13.6</b>	37.44 $\pm$ 2.3	<b>28.02<math>\pm</math>8.6</b>	56.12 $\pm$ 0.3	39.71 $\pm$ 15.0	<b>41.63<math>\pm</math>0.5</b>	37.07
	NAC-ME	<b>50.98<math>\pm</math>8.5</b>	<b>49.65<math>\pm</math>3.5</b>	31.21 $\pm$ 19.0	<b>41.44<math>\pm</math>2.4</b>	27.29 $\pm$ 7.8	<b>57.03<math>\pm</math>0.4</b>	<b>54.33<math>\pm</math>12.7</b>	40.59 $\pm$ 0.9	<b>40.95</b>
ViT-b16	Oracle	-	52.03 $\pm$ 0.3	-	27.35 $\pm$ 3.0	-	49.41 $\pm$ 0.4	-	35.50 $\pm$ 0.3	-
	Validation	<b>21.24<math>\pm</math>11.8</b>	43.51 $\pm$ 2.8	13.15 $\pm$ 4.0	20.85 $\pm$ 2.1	20.02 $\pm$ 18.6	46.55 $\pm$ 0.1	<b>36.44<math>\pm</math>14.2</b>	34.20 $\pm$ 0.7	22.71
	NAC-ME	20.10 $\pm$ 12.4	<b>44.15<math>\pm</math>3.4</b>	<b>17.97<math>\pm</math>1.8</b>	<b>23.43<math>\pm</math>1.0</b>	<b>21.08<math>\pm</math>18.5</b>	<b>47.49<math>\pm</math>0.5</b>	36.11 $\pm$ 16.1	<b>34.80<math>\pm</math>0.6</b>	<b>23.82</b>
ViT-b16	Oracle	-	62.23 $\pm$ 0.4	-	46.69 $\pm$ 1.9	-	56.55 $\pm$ 0.4	-	41.77 $\pm$ 0.3	-
	Validation	-1.31 $\pm$ 3.1	53.13 $\pm$ 2.0	-16.91 $\pm$ 13.4	<b>36.78<math>\pm</math>2.2</b>	-3.27 $\pm$ 9.5	54.19 $\pm$ 0.2	25.16 $\pm$ 7.0	<b>37.84<math>\pm</math>0.4</b>	0.92
	NAC-ME	<b>32.68<math>\pm</math>13.5</b>	<b>57.95<math>\pm</math>2.3</b>	<b>22.39<math>\pm</math>9.4</b>	35.40 $\pm$ 1.6	<b>51.31<math>\pm</math>3.5</b>	<b>55.00<math>\pm</math>0.6</b>	<b>33.01<math>\pm</math>1.4</b>	37.68 $\pm$ 1.6	<b>34.84</b>

Table 16: OOD generalization results on TerraInc dataset [7]. *Oracle* indicates the upper bound. The training strategy is ERM [64]. All scores are averaged over 3 random trials.